Long-Term Scheduling and Power Control for Wirelessly Powered Cell-Free IoT

Xinhua Wang[®], Member, IEEE, Xiaodong Wang[®], Fellow, IEEE, and Alexei Ashikhmin[®], Fellow, IEEE

Abstract—We investigate the long-term scheduling and power control scheme for a wirelessly powered cell-free Internet-of-Things (IoT) network which consists of distributed access points (APs) and a large number of sensors. In each time slot, a subset of sensors is scheduled for uplink data transmission or downlink power transfer. Through asymptotic analysis, we obtain closedform expressions for the harvested energy and the achievable rates that are independent of random pilots. Then, using these expressions, we formulate a long-term scheduling and power control problem to maximize the minimum time-average achievable rate among all sensors while maintaining the battery state of each sensor higher than a predefined minimum level. Using Lyapunov optimization, the transmission mode, the active sensor set, and the power control coefficients for each time slot are jointly determined. Finally, simulation results validate the accuracy of our derived closed-form expressions and reveal that the minimum time-average achievable rate is boosted significantly by the proposed scheme compared with the simple greedy transmission scheme.

Index Terms—Cell-free Internet of Things (IoT), long-term scheduling and power control, Lyapunov optimization, max-min fairness, wireless power transfer (WPT).

I. INTRODUCTION

OWDAYS, the Internet of Things (IoT) has become a ubiquitous technology with wide applications on transportation, healthcare, agriculture, and other aspects of our daily life [1], [2]. The limited energy storage of IoT devices [3] and massive connectivity [4] are two main challenges to hinder the proliferation of IoT technologies and have attracted intensive research interests in recent years [5].

A. Related Work

Wireless power transfer (WPT) is regarded as a promising technology to tackle the energy shortage problem of IoT devices. WPT has been mainly considered for three

Manuscript received April 20, 2020; revised May 29, 2020; accepted June 16, 2020. Date of publication June 19, 2020; date of current version December 21, 2020. This work was supported in part by the Natural Science Foundation of Shandong under Grant ZR2017MF066; in part by the U.S. National Science Foundation under Grant CCF1814803; and in part by the National Natural Science Foundation of China under Grant 61561046. (Corresponding author: Xinhua Wang.)

Xinhua Wang is with the College of Electrical Engineering, Qingdao University, Qingdao 266071, China (e-mail: xhwang@qdu.edu.cn).

Xiaodong Wang is with the Electrical Engineering Department, Columbia University, New York, NY 10027 USA (e-mail: wangx@ee.columbia.edu).

Alexei Ashikhmin is with the Mathematics and Algorithms of Communications Department, Nokia Bell Labs, Murray Hill, NJ 07974 USA (e-mail: alexei.ashikhmin@nokia-bell-labs.com).

Digital Object Identifier 10.1109/JIOT.2020.3003646

scenarios: 1) energy broadcasting without information transmission [6], [7]; 2) simultaneous wireless information and power transfer (SWIPT) [8], [9]; and 3) the wireless powered communication network (WPCN), which is more suitable for IoT [10], [11]. In WPCN, IoT devices first harvest RF energy from the downlink and then transmit data to access points (APs) through the uplink. Although multiple antennas can improve the efficiency of WPT [12], the performance of cell-boundary users is still poor, which results from the heavy path loss in both the downlink WPT phase and the uplink data transmission phase.

Recently, cell-free massive MIMO with distributed and cooperative APs has been proposed to improve both the spectral and energy efficiencies. Compared with cellular massive MIMO, the heavy path loss of the cell boundary terminals can be avoided since the distances between the terminals and served APs are smaller. With the help of cell-free massive MIMO with a user-centric architecture [13], [14], Wang *et al.* [15] proposed a wirelessly powered cell-free IoT scheme with jointly optimized downlink and uplink power control coefficients. Compared with WPT in small cells and collocated massive MIMOs, the WPT efficiency of the cell-free IoT has been improved significantly.

In cell-free massive MIMO systems, random pilots are wildly adopted since it is impossible to allocate finite orthogonal pilots to massive amounts of sensors [15], [16]. Due to the nonorthogonality of random pilots, the channel estimate is degraded by pilot signals transmitted from other users [13]. That is, the nonorthogonal random pilots will reduce the accuracy of channel estimation and further decrease the efficiency of WPT and data transmission. Therefore, user scheduling is critical to satisfy the massive connections in wirelessly powered cell-free IoT. The traditional scheduling methods usually focus on improving the instantaneous network performance [17], [18], which may cause some sensors with bad channel conditions never scheduled.

Motivated by this fact, we aim to design a long-term scheduling strategy to serve more sensors in the wirelessly powered cell-free IoT network. The Lyapunov optimization method is an effective way to improve the infinite horizon average objective function without predicting the future state [19], [20], which has been used to design scheduling strategies in some works [20], [21]. In particular, with the help of Lyapunov optimization, Zhai *et al.* [21] designed an energy-efficient user scheduling for NOMA-based IoT networks to minimize the time-average power consumption while satisfying the time-average rate requirements for all devices.

2327-4662 © 2020 IEEE. Personal use is permitted, but republication/redistribution requires IEEE permission. See https://www.ieee.org/publications/rights/index.html for more information.

Through optimizing energy beamforming, Choi and Kim [22] minimized the time-average power consumption of the AP while meeting the given time-average rate requirements for all nodes in a WPCN.

B. Contribution

To serve more sensors, we investigate the long-term scheduling and power control scheme for a wirelessly powered cell-free IoT network. Our contributions in this work are threefold.

- We provide an asymptotic analysis to obtain closed-form expressions for the harvested energy and the achievable rates that are independent of random pilot sequences.
- 2) To serve massive amounts of sensors, a long-term scheduling and power control optimization problem is formulated to maximize the minimum time-average achievable rate while maintaining the battery state of each sensor higher than a predefined level. By solving the problem, the transmission mode (energy harvesting or data transmission), the active sensor set, and the power control coefficients for each time slot are jointly determined.
- 3) Under the Lyapunov optimization framework, the long-term problem is transformed into a sequence of optimization problems of minimizing the Lyapunov drift plus penalty for each time slot, which can be solved efficiently using our proposed low-complexity methods. The simulation results reveal that our scheduling and power control scheme can boost the minimum time-average achievable rate significantly.

Different from previous works on WPT [23], we investigate the wirelessly powered cell-free IoT with nonorthogonal random pilots. Due to the nonorthogonal pilots, the estimates of channel vectors between different sensors and the same AP are dependent, which leads to challenges for deriving the asymptotic expressions for the harvested energy and the achievable rates. Compared with previous scheduling schemes such as [24], it is challenging to jointly design the long-term scheduling and power control scheme for a wirelessly powered network, since we need to strike a balance between the WPT and data transmission and to guarantee the fairness among sensors.

The remainder of this article is organized as follows. In Section II, we describe the system model and formulate the problem. The asymptotic analysis is provided in Section III. In Section IV, we transform the long-term scheduling and power control problem into Lyapunov optimization. The algorithm for solving the uplink and downlink subproblems in each time slot is described in Section V. The simulation results are given in Section VI. Finally, Section VII concludes the article.

II. SYSTEM MODEL AND OUTLINE OF RESULTS

A. System Model

We consider a wirelessly powered cell-free IoT network [15] with L APs and a set of randomly distributed single-antenna sensors denoted as K with |K| = K. Each AP equipped with N antennas is connected to a central processing unit (CPU) via

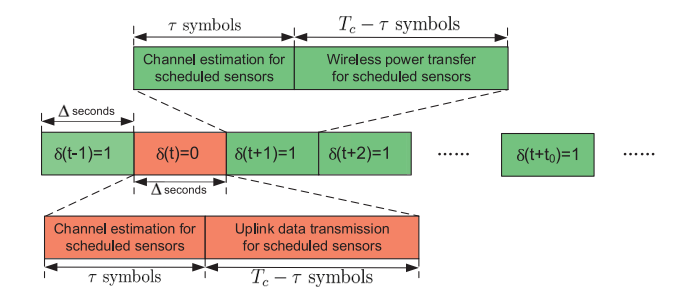


Fig. 1. Scheduling for cell-free IoT.

a perfect back-haul network. In each time slot t, only a subset $\mathcal{K}_a^{(t)}$ with $|\mathcal{K}_a^{(t)}| = K_a$ are scheduled as active sensors while the remaining sensors are inactive. As shown in Fig. 1, each time slot of duration Δ seconds contains T_c orthogonal frequency-division multiplexing (OFDM) symbols, in which τ OFDM symbols are used for channel estimation, while the remaining $T_c - \tau$ symbols are used for downlink WPT if $\delta^{(t)} = 1$ or uplink data transmission if $\delta^{(t)} = 0$, where

$$\delta^{(t)} = \{0, 1\}, \quad t = 0, 1, 2, \dots \tag{1}$$

indicates the transmission mode with $\bar{\delta}^{(t)} = 1 - \delta^{(t)}$.

Let $\boldsymbol{\theta}^{(t)} = [\theta_1^{(t)}, \dots, \theta_K^{(t)}]^T$ denote the sensor states in time slot t with

$$\left|\boldsymbol{\theta}^{(t)}\right|_{1} = K_a, \text{ and } \theta_k^{(t)} \in \{0, 1\}, k \in \mathcal{K}$$
 (2)

i.e., the set of active sensors is $\mathcal{K}_a^{(t)} = \{k : \theta_k^{(t)} = 1\}$. The channel between the *k*th sensor and the *n*th antenna of the *l*th AP in time slot *t* is

$$g_{(l,n),k}^{(t)} = \sqrt{\beta_{l,k}} h_{(l,n),k}^{(t)}$$

where $\beta_{l,k}$ is the large-scale fading coefficient, which depends on the location and is assumed known to the APs. $h_{(l,n),k}^{(t)} \sim \mathcal{CN}(0,1)$ represents the small-scale fading coefficient, which remains invariant in each time slot, but varies independently from one slot to another. The channel between the *l*th AP and the *k*th sensor is denoted as

$$\boldsymbol{g}_{l,k}^{(t)} = \left[g_{(l,1),k}^{(t)}, \dots, g_{(l,N),k}^{(t)}\right]^T \in \mathbb{C}^{N \times 1}$$

while the channel between the *n*th antenna of *l*th AP and all sensors is denoted as

$$\boldsymbol{g}_{(l,n)}^{(t)} = \left[g_{(l,n),1}^{(t)}, \dots, g_{(l,n),K}^{(t)}\right]^T \in \mathbb{C}^{K \times 1}.$$

B. Channel Estimation Phase

At the channel estimation phase in each time slot, all K_a active sensors simultaneously transmit their pilot sequences to APs. Let $\Psi = [\psi_1, \dots, \psi_K] \in \mathbb{C}^{\tau \times K}$, where $\psi_k \sim \mathcal{CN}(\mathbf{0}, [1/\tau] I_\tau)$ denotes the pilot sequence of the kth sensor. In the tth slot, the received pilots at the tth antenna of the tth AP is given by

$$\mathbf{y}_{(l,n)}^{(t)} = \sqrt{\tau \rho_p} \sum_{k=1}^{K} \theta_k^{(t)} g_{(l,n),k}^{(t)} \boldsymbol{\psi}_k + \boldsymbol{w}_{(l,n)}^{(t)}$$
$$= \sqrt{\tau \rho_p} \boldsymbol{\Psi} \boldsymbol{\Theta}^{(t)} \boldsymbol{g}_{(l,n)}^{(t)} + \boldsymbol{w}_{(l,n)}^{(t)} \in \mathbb{C}^{\tau \times 1}$$
(3)

where $\mathbf{w}_{(l,n)}^{(t)} \sim \mathcal{CN}(\mathbf{0}, \sigma^2 \mathbf{I}_{\tau})$ is the additive noise at the *n*th antenna of the *l*th AP, ρ_p is the pilot transmit power, and $\mathbf{\Theta}^{(t)} = \mathrm{diag}(\mathbf{\theta}^{(t)})$ is the diagonal matrix indicating the sensor states. Using the received pilots $\mathbf{y}_{(l,n)}^{(t)}$, the LMMSE channel estimate $\hat{\mathbf{g}}_{(l,n)}^{(t)}$ is given by

$$\hat{oldsymbol{g}}_{(l,n)}^{(t)} = \left[oldsymbol{A}_{l}^{(t)}
ight]^{H} oldsymbol{y}_{(l,n)}^{(t)}$$

which implies that the kth entry of $\hat{g}_{(l,n)}$ is

$$\hat{g}_{(l,n),k}^{(t)} = \left[\mathbf{a}_{l,k}^{(t)} \right]^{H} \mathbf{y}_{(l,n)}^{(t)}$$
(4)

where

$$\boldsymbol{A}_{l}^{(t)} = \sqrt{E_{p}} \left(\boldsymbol{I}_{\tau} + E_{p} \boldsymbol{\Psi} \boldsymbol{D}_{l}^{(t)} \boldsymbol{\Psi}^{H} \right)^{-1} \boldsymbol{\Psi} \boldsymbol{D}_{l}^{(t)}.$$

 $E_p = \tau \rho_p / \sigma^2$, $\boldsymbol{D}_l^{(t)} = \operatorname{diag}(\beta_{l,1}, \dots, \beta_{l,K}) \boldsymbol{\Theta}^{(t)}$, and $\boldsymbol{a}_{l,k}^{(t)}$ is the kth column of $\boldsymbol{A}_l^{(t)}$. Define

$$\mathbf{Z}_{l}^{(t)} = \mathbf{I}_{\tau} + E_{p} \mathbf{\Psi} \mathbf{D}_{l}^{(t)} \mathbf{\Psi}^{H}$$

$$= \mathbf{I}_{\tau} + \sum_{j \in \mathcal{K}_{a}^{(t)}} E_{p} \beta_{l,j} \mathbf{\psi}_{j} \mathbf{\psi}_{j}^{H}.$$
(5)

The mean squared value of the channel estimate $\hat{g}_{(l,n),k}^{(t)}$ is given by

$$\gamma_{l,k}^{(t)} = \mathbb{E}\left[\left|\hat{\mathbf{g}}_{(l,n),k}^{(t)}\right|^{2}\right] = \left[\mathbb{E}\left(\hat{\mathbf{g}}_{(l,n)}^{(t)}\left[\hat{\mathbf{g}}_{(l,n)}^{(t)}\right]^{H}\right)\right]_{kk} \\
= \sqrt{\tau \rho_{p}} \beta_{l,k} \boldsymbol{\psi}_{k}^{H} \boldsymbol{a}_{l,k}^{(t)} \\
= \tau \rho_{p} \beta_{l,k}^{2} \boldsymbol{\psi}_{k}^{H} \left[\boldsymbol{Z}_{l}^{(t)}\right]^{-1} \boldsymbol{\psi}_{k}, \quad k \in \mathcal{K}_{a}^{(t)}. \tag{6}$$

C. Tranmission Phase

1) Downlink WPT: If $\delta^{(t)} = 1$, during the remaining $T_c - \tau$ symbols, the APs jointly perform energy beamforming to the active sensors based on channel estimates, i.e., the transmitted signal from the lth AP within the ℓ th OFDM symbol is

$$\mathbf{x}_{l}^{(t,\ell)} = \sqrt{\rho_{d}} \sum_{j=1}^{K} \sqrt{\eta_{l,j}^{(t)} \theta_{j}^{(t)}} \left[\hat{\mathbf{g}}_{l,j}^{(t)} \right]^{*} q_{j}^{(t,\ell)}, \, \ell = \tau + 1, \dots, T_{c} \quad (7)$$

where $q_j^{(t,\ell)} \sim \mathcal{CN}(0, 1/(T_c - \tau))$ is the ℓ th symbol to the jth sensor, and

$$\eta_{l,i}^{(t)} \ge 0 \quad \forall l, j \tag{8}$$

denote the downlink power control coefficients. The transmit power of each AP is constrained by

$$P_{l}^{(t)} = \sum_{\ell=\tau+1}^{T_{c}} \mathbb{E}\left[\left\|\boldsymbol{x}_{l}^{(t,\ell)}\right\|^{2}\right] \leq N\rho_{d} \quad \forall l$$
 (9)

where $N\rho_d$ is the maximum transmit power of each AP. Substituting (6) and (7) into (9), we have

$$\sum_{k=1}^{K} \delta^{(t)} \theta_k^{(t)} \eta_{l,k}^{(t)} \gamma_{l,k}^{(t)} \le 1 \quad \forall l.$$
 (10)

Then, the received signal at the kth sensor is

$$z_k^{(t,\ell)} = \sum_{l=1}^{L} \left[\mathbf{g}_{l,k}^{(t)} \right]^T \mathbf{x}_l^{(t,\ell)} + v_k^{(t,\ell)}, \quad \ell = \tau + 1, \dots, T_c$$
(11)

where $v_k^{(t)} \sim \mathcal{CN}(0, \sigma^2/(T_c - \tau))$ is the noise. The amount of harvested energy at the each active sensor during each time slot can be expressed as

$$\mathcal{E}_k^{(t)} = (1 - \alpha) \Delta \zeta \delta^{(t)} \theta_k^{(t)} (T_c - \tau) \mathbb{E} \left[\left| z_k^{(t,\ell)} \right|^2 \right]$$
 (12)

where $\alpha = \tau/T_c$ and $\zeta \in (0, 1)$ represents the energy conversion efficiency.

2) Uplink Data Transmission: If $\delta^{(t)} = 0$, during the remaining $T_c - \tau$ symbols, K_a active sensors simultaneously deliver their data to APs. The received signal at the *l*th AP within the ℓ th OFDM symbol is given by

$$\boldsymbol{r}_{l}^{(t,\ell)} = \sqrt{\rho_{u}} \sum_{j=1}^{K} \sqrt{\xi_{j}^{(t)} \theta_{j}^{(t)}} \boldsymbol{g}_{l,j}^{(t)} s_{j}^{(t,\ell)} + \boldsymbol{n}_{l}^{(t,\ell)}$$

where $s_j^{(t,\ell)}$ denotes the ℓ th uplink symbol of the jth sensor with $\mathbb{E}[|s_j^{(t,\ell)}|^2] = 1/(T_c - \tau)$, ρ_u is the maximum transmit power of each sensor, $\boldsymbol{n}_l^{(t,\ell)} \sim \mathcal{CN}(\boldsymbol{0}, [\sigma^2/(T_c - \tau)]\boldsymbol{I}_N)$ is the additive noise, and $\xi_k^{(t)}$ represents the power control coefficient of the kth sensor with

$$0 \le \xi_k^{(t)} \le 1, \quad k \in \mathcal{K}. \tag{13}$$

The energy consumption of each active sensor for data transmission in each time slot is

$$E_k^{(t)} = (1 - \alpha) \Delta \rho_u \theta_k^{(t)} \xi_k^{(t)} \le b_k^{(t)}, \quad k \in \mathcal{K}$$
 (14)

where $b_k^{(t)}$ is the battery state of the kth sensor at the beginning of time slot t. Each AP individually performs beamforing and then sends $\hat{g}_{l,k}^H r_l^{(t,\ell)}$ to the CPU, which detects $s_k^{(t,\ell)}$ using matched filtering (MF) as follows:

$$\hat{\boldsymbol{s}}_{k}^{(t,\ell)} = \sum_{l=1}^{L} \left[\hat{\boldsymbol{g}}_{l,k}^{(t)} \right]^{H} \boldsymbol{r}_{l}^{(t,\ell)} = \underbrace{\sqrt{\rho_{u} \boldsymbol{\xi}_{k}^{(t)}}}_{C_{1}} \sum_{l=1}^{L} \mathbb{E} \left[\left[\hat{\boldsymbol{g}}_{l,k}^{(t)} \right]^{H} \boldsymbol{g}_{l,k}^{(t)} \right] \boldsymbol{s}_{k}^{(t,\ell)}$$

$$+ \underbrace{\sqrt{\rho_{u} \boldsymbol{\xi}_{k}^{(t)}}}_{L=1} \sum_{l=1}^{L} \left(\left[\hat{\boldsymbol{g}}_{l,k}^{(t)} \right]^{H} \boldsymbol{g}_{l,k}^{(t)} - \mathbb{E} \left[\left[\hat{\boldsymbol{g}}_{l,k}^{(t)} \right]^{H} \boldsymbol{g}_{l,k}^{(t)} \right] \right) \boldsymbol{s}_{k}^{(t,\ell)}$$

$$+ \underbrace{\sum_{j \neq k, j \in \mathcal{K}}}_{C_{2}} \sqrt{\rho_{u} \boldsymbol{\xi}_{j}^{(t)} \boldsymbol{\theta}_{j}^{(t)}} \sum_{l=1}^{L} \left[\hat{\boldsymbol{g}}_{l,k}^{(t)} \right]^{H} \boldsymbol{g}_{l,j}^{(t)} \boldsymbol{s}_{j}^{(t,\ell)}$$

$$+ \underbrace{\sum_{l=1}^{L} \left[\hat{\boldsymbol{g}}_{l,k}^{(t)} \right]^{H} \boldsymbol{n}_{l}^{(t,\ell)}}_{L}$$

where C_1 is the desired signal, and $C_2 + C_3 + C_4$ is the effective noise. Since C_1 , C_2 , C_3 , and C_4 are uncorrelated, the achievable rate of the *k*th sensor is lower bounded by [13], [14]

$$R_k^{(t)} = (1 - \alpha)\bar{\delta}^{(t)}\theta_k^{(t)}\log_2(1 + \Gamma_k^{(t)})$$
 b/s/Hz (15)

where the effective SINR Γ_k is

$$\Gamma_k^{(t)} = \frac{|\mathcal{C}_1|^2}{\mathbb{E}[|\mathcal{C}_2|^2] + \mathbb{E}[|\mathcal{C}_3|^2] + \mathbb{E}[|\mathcal{C}_4|^2]}$$
(16)

where the expectation is taken over small-scale fading.

3) Battery Model: Let b_{\max} denote the capacity of the battery. Since $b_k^{(t)} - E_k^{(t)} \ge 0$ from (14), the battery state of the kth sensor $b_k^{(t)}$ is updated at the beginning of each time slot according to

$$b_k^{(t+1)} = \min \left\{ b_k^{(t)} - \bar{\delta}^{(t)} E_k^{(t)} + \delta^{(t)} \mathcal{E}_k^{(t)}, b_{\text{max}} \right\}. \tag{17}$$

From (14), in order to guarantee certain minimum data rate, we constrain the battery state of each sensor at the beginning of each time slot to be above a predefined threshold b_0 , i.e.,

$$b_k^{(t)} \ge b_0, \quad k \in \mathcal{K}. \tag{18}$$

D. Outline of Results

Note that the quantities $\gamma_{l,k}^{(t)}$, $\mathcal{E}_k^{(t)}$, and $R_k^{(t)}$ given in (6), (11), and (15) are functions of the random pilot sequences Ψ . In Section III, an asymptotic analysis is performed as $\tau \to \infty$ while keeping α , $\kappa = \tau/K_a$, and E_p fixed, which shows that $\gamma_{l,k}$, $\tilde{\mathcal{E}}_k(t)$, and $R_k(t)$ become independent of Ψ in this regime, i.e.,

$$\begin{split} & \gamma_{l,k}^{(t)} - \bar{\gamma}_{l,k}^{(t)} \xrightarrow{\text{a.s.}} 0, \quad k \in \mathcal{K}, l = 1, \dots, L \\ & \tilde{\mathcal{E}}_k^{(t)} - \bar{\mathcal{E}}_k^{(t)} \xrightarrow{\text{a.s.}} 0, \quad k \in \mathcal{K} \\ & R_k^{(t)} - \bar{R}_k^{(t)} \xrightarrow{\text{a.s.}} 0, \quad k \in \mathcal{K} \end{split}$$

where $\tilde{\mathcal{E}}_k^{(t)}$ is a tight lower bound of $\mathcal{E}_k^{(t)}$. The closed-form expressions of $\bar{\gamma}_{l,k}^{(t)}$, $\bar{\mathcal{E}}_k^{(t)}$, and $\bar{R}_k^{(t)}$ (that are independent of Ψ) can be used to predict the performance of the general case with large but finite length of pilot.

In Section IV, we consider a long-term scheduling and power control problem to maximize the minimum time-averaged achievable rate $\min_{k \in \mathcal{K}} \lim_{T \to \infty} (1/T) \sum_{t=0}^{T-1} \bar{\delta}^{(t)} R_k^{(t)}$ while meeting all the constraints detailed in Section II-A. Specifically, given the large-scale fading coefficients $\{\beta_{l,k}\}$, the overall policy in time slot t consists of the transmission mode $\delta^{(t)}$, sensor states $\boldsymbol{\theta}^{(t)}$, downlink power control coefficients $\boldsymbol{\eta}^{(t)}$, and uplink power control coefficients $\boldsymbol{\xi}^{(t)}$, i.e.,

$$\mathcal{P}^{(t)} = \left\{ \delta^{(t)}, \boldsymbol{\theta}^{(t)}, \boldsymbol{\eta}^{(t)}, \boldsymbol{\xi}^{(t)} \right\} \tag{19}$$

and the long-term optimization problem is formulated as

$$\mathbf{P}_{1}: \max_{\{\mathcal{P}^{(t)}\}} \min_{k \in \mathcal{K}} \lim_{T \to \infty} \frac{1}{T} \sum_{t=0}^{T-1} R_{k}^{(t)}$$
s.t. (1), (2), (8), (10), (13), (14), (17), (18). (20)

In general, \mathbf{P}_1 is NP-hard due to the following reasons. First, it is a max-min problem with an infinite horizon average objective function. Second, the constraint region is also over infinite horizon. In addition, it is a mixed integer program due to the 0-1 constraints with respect to (w.r.t.) the sensor states.

To overcome these difficulties, in Section IV, we first relax P_1 into a maximization problem P_2 with long-term

constraints. Through establishing virtual queues, \mathbf{P}_2 is then reformulated into a maximization problem \mathbf{P}_2' with the constraints on the rate stability of virtual queues. Using Lyapunov optimization, problem \mathbf{P}_2' is then decomposed into a sequence of optimization problems of minimizing the Lyapunov drift plus penalty for each time slot. To solve the problem for each time slot, in Section V, we propose two low-complexity optimization methods for the downlink WPT and the uplink data transmission, respectively.

III. Asymptotic Analysis as $\tau \to \infty$

Based on (5), denote

$$\begin{aligned} \boldsymbol{Z}_{l,k}^{(t)} &= \boldsymbol{Z}_{l}^{(t)} - E_{p} \beta_{l,k} \boldsymbol{\psi}_{k} \boldsymbol{\psi}_{k}^{H} \\ &= \boldsymbol{I}_{\tau} + \sum_{j \in \mathcal{K}_{a}^{(t)}/\{k\}} E_{p} \beta_{l,j} \boldsymbol{\psi}_{j} \boldsymbol{\psi}_{j}^{H} \\ &= \boldsymbol{I}_{\tau} + \boldsymbol{\Xi}_{l,k} \boldsymbol{\Xi}_{l,k}^{H} \end{aligned}$$

where $\mathbf{\Xi}_{l,k} = \mathbf{\Psi}_k \mathbf{\Sigma}_{l,k}^{(1/2)}$, with $\mathbf{\Psi}_k = (, \dots, \mathbf{\psi}_j, \dots)$, and $\mathbf{\Sigma}_{l,k} = \operatorname{diag}(, \dots, E_p \beta_{l,j}, \dots)$ with $j \in \mathcal{K}_a^{(t)}/\{k\}$. Then, it is straightforward to obtain the following lemma according to [26, Th. 1 and 2].

Lemma 1: As $\tau \to \infty$, we have

$$\operatorname{tr}\left[\left(\mathbf{Z}_{l,k}^{(t)}\right)^{-1}\right]/\tau - \mathcal{Z}_{l,k}^{(t)} \xrightarrow{\text{a.s.}} 0, \tag{21}$$

$$\operatorname{tr}\left[\left(\mathbf{Z}_{l,k}^{(t)}\right)^{-2}\right]/\tau - \tilde{\mathcal{Z}}_{l,k}^{(t)} \xrightarrow{\text{a.s.}} 0. \tag{22}$$

 $\mathcal{Z}_{lk}^{(t)}$ is given as

$$\mathcal{Z}_{l,k}^{(t)} = \left[\sum_{j \in \mathcal{K}_a^{(t)}/\{k\}} \frac{E_p \beta_{l,j}}{\tau \left(1 + \varsigma_j\right)} + 1 \right]^{-1}$$

and $\boldsymbol{\varsigma} = [\ldots, \varsigma_j, \ldots,]^T, j \in \mathcal{K}_a^{(t)}/\{k\}$ is the unique solution to the following set of fixed-point equations:

$$\varsigma_{j} = E_{p}\beta_{l,j} \left[\sum_{j \in \mathcal{K}_{a}^{(l)}/\{k\}} \frac{E_{p}\beta_{l,j}}{\tau \left(1 + \varsigma_{j}\right)} + 1 \right]^{-1}$$

with initial values $\varsigma_j = 1$. $\tilde{\mathcal{Z}}_{l,k}^{(t)}$ is given as

$$\tilde{\mathcal{Z}}_{l,k}^{(t)} = \left[1 + \frac{1}{\tau} \sum_{j \in \mathcal{K}_a^{(t)}/\{k\}} \frac{E_p \beta_{l,j} \hat{S}_j}{(1+\varsigma_j)^2} \right] \left[\mathcal{Z}_{l,k}^{(t)}\right]^{-2}$$

and $\hat{\boldsymbol{\varsigma}} = [\ldots, \hat{\varsigma}_j, \ldots,]^T, j \in \mathcal{K}_a^{(t)}/\{k\}$ is given by

$$\hat{\boldsymbol{\varsigma}} = (\boldsymbol{I}_{(K_a - 1)} - \boldsymbol{J})^{-1} \boldsymbol{c}$$

$$[\boldsymbol{J}]_{j,i} = \frac{E_p^2 \beta_{l,j} \beta_{l,i}}{\tau (1 + \varsigma_j)^2} \left[\mathcal{Z}_{l,k}^{(t)} \right]^{-2}$$

$$[\boldsymbol{c}]_j = E_p \beta_{l,j} \left[\mathcal{Z}_{l,k}^{(t)} \right]^{-2}.$$

A. Asymptotic Analysis of $\gamma_{lk}^{(t)}$

Theorem 1: As $\tau \to \infty$, the mean-squared value of channel estimate given in (6) almost surely converges to a deterministic

value independent of the random pilots Ψ , i.e.,

$$\gamma_{l,k}^{(t)} - \bar{\gamma}_{l,k}^{(t)} \xrightarrow{\text{a.s.}} 0, \quad k \in \mathcal{K}_a^{(t)}$$
(23)

where

$$\bar{\gamma}_{l,k}^{(t)} = \frac{E_p \beta_{l,k}^2 \mathcal{Z}_{l,k}^{(t)}}{1 + E_p \beta_{l,k} \mathcal{Z}_{l,k}^{(t)}}.$$
(24)

Proof: See Appendix A.

B. Asymptotic Analysis of $\mathcal{E}_k^{(t)}$

To analyze $\mathcal{E}_k^{(t)}$ in (12), we first introduce the following lemma from [15] on the LMMSE channel estimation with random pilots.

Lemma 2: For $m, l \in \{1, ..., L\}$ with $m \neq l$ and $k \in \mathcal{K}_a^{(t)}$, we have

$$\operatorname{cov}\left[\hat{\boldsymbol{g}}_{l,k}^{(t)},\ \hat{\boldsymbol{g}}_{m,k}^{(t)}\right] = \mathbf{0}$$
and
$$\operatorname{cov}\left[\left\|\hat{\boldsymbol{g}}_{l,k}^{(t)}\right\|^{2},\ \left\|\hat{\boldsymbol{g}}_{m,k}^{(t)}\right\|^{2}\right] = \mathbf{0}.$$

Lemma 2 reveals that the channel estimates between different APs and a sensor are uncorrelated. However, the channel estimates between an AP and different sensors are correlated, since $\hat{g}_{(l,n),k}^{(t)}$ depends on $g_{(l,n),j}^{(t)}$ and ψ_j with $j \in \mathcal{K}_a^{(t)}$, which can be seen from (3) and (4). Since the channel estimation error $\tilde{\mathbf{g}}_{l,k}^{(t)} = \mathbf{g}_{l,k}^{(t)} - \hat{\mathbf{g}}_{l,k}^{(t)}$ is independent of $\hat{\mathbf{g}}_{l,k}^{(t)}$, $z_k^{(t,\ell)}$ in (11) can be rewritten as

$$\begin{split} z_k^{(t,\ell)} &= \sum_{l=1}^L \left[\hat{\mathbf{g}}_{l,k}^{(t)} \right]^T \mathbf{x}_l^{(t,\ell)} + \sum_{l=1}^L \left[\tilde{\mathbf{g}}_{l,k}^{(t)} \right]^T \mathbf{x}_l^{(t,\ell)} + v_k^{(t,\ell)} \\ &= \underbrace{\sum_{l=1}^L \sqrt{\rho_d \eta_{l,k}^{(t)} \theta_k^{(t)}} \left[\hat{\mathbf{g}}_{l,k}^{(t)} \right]^T \left[\hat{\mathbf{g}}_{l,k}^{(t)} \right]^* q_k^{(t,\ell)}}_{S_{k1}} \\ &+ \underbrace{\sum_{l=1}^L \sum_{j \neq k} \sqrt{\rho_d \eta_{l,j}^{(t)} \theta_j^{(t)}} \left[\hat{\mathbf{g}}_{l,k}^{(t)} \right]^T \left[\hat{\mathbf{g}}_{l,j}^{(t)} \right]^* q_j^{(t,\ell)} + \sum_{l=1}^L \left[\tilde{\mathbf{g}}_{l,k}^{(t)} \right]^T \mathbf{x}_l^{(t,\ell)} + v_k^{(t,\ell)}}_{S_{k2}}. \end{split}$$

Since S_{k1} and S_{k2} are uncorrelated and zero mean, we have

$$\begin{split} \mathcal{E}_{k}^{(t)} &= (1-\alpha)\Delta\zeta\delta^{(t)}\theta_{k}^{(t)}\rho_{d}(T_{c}-\tau) \\ &\times \mathbb{E}\Big[|\mathcal{S}_{k1}|^{2} + |\mathcal{S}_{k2}|^{2} + 2\Re\{\mathcal{S}_{k1}\mathcal{S}_{k2}\}\Big] \\ &\geq (1-\alpha)\Delta\zeta\delta^{(t)}\theta_{k}^{(t)}\rho_{d}(T_{c}-\tau)\mathbb{E}\Big[|\mathcal{S}_{k1}|^{2}\Big] \\ &= (1-\alpha)\Delta\zeta\delta^{(t)}\theta_{k}^{(t)}\rho_{d}\mathbb{E}\Bigg[\left|\sum_{l=1}^{L}\sqrt{\eta_{l,k}^{(t)}}[\hat{\mathbf{g}}_{l,k}]^{T}[\hat{\mathbf{g}}_{l,k}^{(t)}]^{*}\Big|^{2}\Big] \\ &= (1-\alpha)\Delta\zeta\delta^{(t)}\theta_{k}^{(t)}\rho_{d}\\ &\times \mathbb{E}\Bigg[\sum_{l=1}^{L}\sum_{m=1}^{L}\sqrt{\eta_{l,k}^{(t)}\eta_{m,k}^{(t)}}[\hat{\mathbf{g}}_{l,k}^{(t)}]^{T}[\hat{\mathbf{g}}_{l,k}^{(t)}]^{*}[\hat{\mathbf{g}}_{m,k}^{(t)}]^{T}[\hat{\mathbf{g}}_{m,k}^{(t)}]^{*}\Big] \\ &\stackrel{(a)}{=} (1-\alpha)\Delta\zeta\delta^{(t)}\theta_{k}^{(t)}\rho_{d}N\Bigg[N\Bigg(\sum_{l=1}^{L}\sqrt{\eta_{l,k}^{(t)}}\gamma_{l,k}^{(t)}\Bigg)^{2} \\ &+\sum_{l=1}^{L}\eta_{l,k}^{(t)}\Big[\gamma_{l,k}^{(t)}\Big]^{2}\Bigg] \end{split}$$

$$\geq \tilde{\mathcal{E}}_{k}^{(t)} \triangleq (1 - \alpha) \Delta \zeta \delta^{(t)} \theta_{k}^{(t)} \rho_{d} N^{2} \left(\sum_{l=1}^{L} \sqrt{\eta_{l,k}^{(t)}} \gamma_{l,k}^{(t)} \right)^{2} \tag{25}$$

where step (a) is obtained according to Lemma 2 and $\mathbb{E}[||\hat{\mathbf{g}}_{l,k}^{(t)}||^4] = N(N+1)[\gamma_{l,k}^{(t)}]^2$. It is straightforward to prove that $\tilde{\mathcal{E}}_k^{(t)} \to \mathcal{E}_k^{(t)}$ as $N \to \infty$, which implies $\tilde{\mathcal{E}}_k^{(t)}$ is a tight lower bound on $\mathcal{E}_k^{(t)}$ for large N. Substituting (23) into (25), we have

$$\tilde{\mathcal{E}}_k^{(t)} - \bar{\mathcal{E}}_k^{(t)} \xrightarrow{\text{a.s.}} 0$$
, as $\tau \to \infty$, $k \in \mathcal{K}_a^{(t)}$ (26)

where

$$\bar{\mathcal{E}}_k^{(t)} = (1 - \alpha) \Delta \zeta \delta^{(t)} \theta_k^{(t)} \rho_d N^2 \left(\sum_{l=1}^L \sqrt{\eta_{l,k}^{(t)}} \bar{\gamma}_{l,k}^{(t)} \right)^2.$$

C. Asymptotic Analysis of $R_k^{(t)}$

For given pilots Ψ , the SINR in (16) can be expressed as [15]

$$\Gamma_k^{(t)} = \frac{\mathcal{D}_k^{(t)} \xi_k^{(t)}}{\mathcal{U}_k^{(t)} \xi_k^{(t)} + \sum_{j \in \mathcal{K}_k^{(t)}/\{k\}} \mathcal{I}_{k,j}^{(t)} \xi_j^{(t)} + \mathcal{N}_k^{(t)}}$$
(27)

where

$$\mathcal{D}_{k}^{(t)} = \rho_{u} N \left(\sum_{l=1}^{L} \gamma_{l,k}^{(t)} \right)^{2}, \quad \mathcal{U}_{k}^{(t)} = \sum_{l=1}^{L} \rho_{u} \gamma_{l,k}^{(t)} \beta_{l,k}$$
$$\mathcal{N}_{k}^{(t)} = \sigma^{2} \sum_{l=1}^{L} \gamma_{l,k}^{(t)}$$

and

$$\mathcal{I}_{k,j}^{(t)} = \rho_{u} \sum_{l=1}^{L} \beta_{l,j} \left\| \boldsymbol{a}_{l,k}^{(t)} \right\|^{2} + \rho_{u} E_{p} N \left| \sum_{l=1}^{L} \beta_{l,j} \boldsymbol{\psi}_{j}^{H} \boldsymbol{a}_{l,k}^{(t)} \right|^{2} + \rho_{u} E_{p} \sum_{l=1}^{L} \sum_{i=1}^{K} \beta_{l,j} \beta_{l,i} \left| \boldsymbol{\psi}_{i}^{H} \boldsymbol{a}_{l,k}^{(t)} \right|^{2}.$$

Theorem 2: As $\tau \to \infty$, the rate in (15) almost surely converges to a deterministic value independent of the random pilots Ψ , i.e.,

$$R_k^{(t)} - \bar{R}_k^{(t)} \xrightarrow{\text{a.s.}} 0, \quad k \in \mathcal{K}_a^{(t)}$$

where

$$\bar{R}_{k}^{(t)} = (1 - \alpha)\bar{\delta}^{(t)}\theta_{k}^{(t)}\log_{2}\left(1 + \bar{\Gamma}_{k}^{(t)}\right), \quad \text{b/s/Hz}$$

$$\bar{\Gamma}_{k}^{(t)} = \frac{\bar{D}_{k}^{(t)}\xi_{k}^{(t)}}{\bar{U}_{k}^{(t)}\xi_{k}^{(t)} + \sum_{i \in K^{(t)}/Ik}\bar{\mathcal{I}}_{k,i}^{(t)}\xi_{i}^{(t)} + \bar{\mathcal{N}}_{k}^{(t)}}$$
(28)

$$\begin{array}{lll} \bar{D}_{k}^{(t)} &=& N\rho_{u}(\sum_{l=1}^{L}\bar{\gamma}_{l,k}^{(t)})^{2}, & \bar{U}_{k}^{(t)} &=& \sum_{l=1}^{L}\rho_{u}\bar{\gamma}_{l,k}^{(t)}\beta_{l,k},\\ \bar{\mathcal{I}}_{k,j}^{(t)} &=& \rho_{u}\sum_{l=1}^{L}\beta_{l,j}\varrho_{l,k}^{(t)}+\rho_{u}E_{p}\sum_{l=1}^{L}\beta_{l,j}\beta_{l,k}\vartheta_{l,k}^{(t)}, \text{ and } \bar{\mathcal{N}}_{k}^{(t)} &=& \sigma^{2}\sum_{l=1}^{L}\bar{\gamma}_{l,k}^{(t)} \text{ with} \end{array}$$

$$\varrho_{l,k}^{(t)} = \frac{E_p \beta_{l,k}^2 \tilde{\mathcal{Z}}_{l,k}^{(t)}}{\left(1 + E_p \beta_{l,k} \mathcal{Z}_{l,k}^{(t)}\right)^2}$$

$$\vartheta_{l,k}^{(t)} = \frac{E_p \beta_{l,k}^2 \left[\mathcal{Z}_{l,k}^{(t)} \right]^2}{\left(1 + E_p \beta_{l,k} \mathcal{Z}_{l,k}^{(t)} \right)^2}.$$

Proof: See Appendix B.

D. Impact of More Active Sensors

It is noted that $\bar{\gamma}_{l,k}^{(t)}$, $\bar{\mathcal{E}}_k^{(t)}$, and $\bar{R}_k^{(t)}$ are functions of the large-scale fading coefficients of active sensors. We now examine the effect of adding more sensor to the current set $\mathcal{K}_a^{(t)}$ on each sensor $k \in \mathcal{K}_a^{(t)}$. In particular, let $\bar{\gamma}_{l,k}^{(t)}$ be the asymptotic mean-squared value of channel estimate given in (24), and $[\bar{\gamma}_{l,k}^{(t)}]'$ be the corresponding value when the active set becomes $[\mathcal{K}_a^{(t)}]' \supset \mathcal{K}_a^{(t)}$ by activating some inactive sensors in $\mathcal{K}/\mathcal{K}_s^{(t)}$. We have the following result.

Lemma 3:

$$\left[\bar{\gamma}_{l,k}^{(t)}\right]' < \bar{\gamma}_{l,k}^{(t)}, \quad k \in \mathcal{K}_a^{(t)}, \quad l = 1, \dots, L.$$
 (29)

Proof: See Appendix C.

Remark 1: The mean-squared error of the channel estimate is

$$e_{l,k}^{(t)} = \mathbb{E}\left[\left\|g_{(l,n),k}^{(t)} - \hat{g}_{(l,n),k}^{(t)}\right\|^2\right] = \beta_{l,k} - \gamma_{l,k}^{(t)}.$$
 (30)

Lemma 3 reveals that the accuracy of channel estimation is reduced by activating inactive sensors. The reduced $\bar{\gamma}_{l,k}^{(t)}$ further degrades the amount of harvested energy $\bar{\mathcal{E}}_k^{(t)}$ in (26) and the achievable rate $\bar{R}_k^{(t)}$ in (28), since they are both monotonically increasing functions w.r.t. $\bar{\gamma}_{l,k}^{(t)}$. Specifically, the influence on the efficiency of WPT is more pronounced since it is proportional to the square of $\bar{\gamma}_{l,k}^{(t)}$.

IV. LONG-TERM SCHEDULING AND POWER CONTROL

In \mathbf{P}_1 , we aim to achieve the max–min fairness over infinite horizon, which is hard to tackle. Similarly, as in [27], we first introduce a sequence of auxiliary variables $r^{(t)}$ bounded between 0 and r_{max} , where $r_{\text{max}} = \max_{k \in \mathcal{K}} \hat{R}_k^{(t)}$, with

$$\hat{R}_k^{(t)} = (1 - \alpha)\theta_k^{(t)}\log_2\left(1 + \frac{N\rho_u}{\sigma^2}\sum_{l=1}^L \beta_{l,k}\right)$$

i.e., $\hat{R}_k^{(t)}$ is the achievable rate of the *k*th sensor in (28) with full transmit power, perfect channel estimation, and no interference. Then, we have

$$0 \le \max_{k \in \mathcal{K}} R_k^{(t)} \le r_{\max}$$

for any t, which implies

$$0 \le \min_{k \in \mathcal{K}} \lim_{T \to \infty} \frac{1}{T} \sum_{t=0}^{T-1} R_k^{(t)} \le r_{\text{max}}.$$

Thus, the max-min problem \mathbf{P}_1 is equivalent to maximizing $\lim_{T\to\infty}(1/T)\sum_{t=0}^{T-1}r^{(t)}$ with the following two extra constraints [19], [27]:

$$\liminf_{T \to \infty} \frac{1}{T} \sum_{t=0}^{T-1} \left[R_k^{(t)} - r^{(t)} \right] \ge 0, \quad k \in \mathcal{K}$$
 (31)

$$0 \le r^{(t)} \le r_{\text{max}}.\tag{32}$$

Another challenge resides in constraint (18), which makes the control policy $\mathcal{P}^{(t)}$ over different time slots coupled due to the dynamics of $b_k^{(t)}$ in (17). We therefore relax (18) to the following long-term constraint:

$$\liminf_{T \to \infty} \frac{1}{T} \sum_{t=1}^{T-1} b_j^{(t)} \ge b_0, \quad k \in \mathcal{K}$$
(33)

which enable us to design the policy using Lyapunov optimization. Hence, P_1 is relaxed to

$$\mathbf{P}_{2}: \max_{\{\mathcal{P}^{(t)}, r^{(t)}\}} \lim_{T \to \infty} \frac{1}{T} \sum_{t=0}^{T-1} r^{(t)}$$
s.t. (31), (32), (33)
(1), (2), (8), (10), (13), (14), (17).

A. Problem Reformulation With Queue Stability Constraints

 P_2 is still hard to tackle due to the long-term constraints (31) and (33). Similarly, as in [21] and [25], we transform the long-term constraints into queue stability constraints.

Define $\{X_k(t): k \in \mathcal{K}\}$ as the virtual queues associated with constraint (33). In each time slot, the virtual queue $X_k(t)$ is updated according to

$$X_k(t+1) = \left[X_k(t) + b_0 - b_k^{(t+1)}\right]^+ \tag{34}$$

where $[x]^+ = \max\{0, x\}$. b_0 and $b_k^{(t+1)}$ can be considered as the arrival rate and the departure rate of the virtual queue $X_k(t)$, respectively. We say $X_k(t)$ is rate stable if $\lim_{t\to\infty}([X_k(t)]/t) = 0$ [21], [25]. To maintain the rate stability of $X_k(t)$, the departure rate $b_k^{(t+1)}$ must be no less than the arrival rate b_0 , which coincides with constraint (33).

Similarly, we also define $\{Y_k(t): k \in \mathcal{K}\}$ as the virtual queues associated with constraint (31), where $Y_k(t)$ is updated as

$$Y_k(t+1) = \left[Y_k(t) + r^{(t)} - R_k^{(t)}\right]^+. \tag{35}$$

To reveal the relation between the long-term constraints (31) and (33) in \mathbf{P}_2 and the rate stability of $\{X_k(t), Y_k(t) : k \in \mathcal{K}\}$, we have the following lemma.

Lemma 4: If $\{X_k(t), Y_k(t) : k \in \mathcal{K}\}$ are rate stable with finite initial values, then the long-term constraints (31) and (33) are satisfied.

Proof: Without loss of generality, we take $X_k(t)$ for example. Equation (34) can be rewritten as

$$X_k(t+1) = X_k(t) - b_k^{(t+1)} + \max \left\{ b_0, b_k^{(t+1)} - X_k(t) \right\}.$$

Sum over t = 0, ..., T - 1, we have

$$X_{k}(T) - X_{k}(0) = \sum_{t=0}^{T-1} \left\{ \max \left\{ b_{0}, b_{k}^{(t+1)} - X_{k}(t) \right\} - b_{k}^{(t+1)} \right\}$$

$$\geq Tb_{0} - \sum_{t=1}^{T} b_{k}^{(t)}. \tag{36}$$

Dividing both sides of (36) by T and taking the limit, we obtain

$$\lim_{T \to \infty} \inf \frac{X_k(T)}{T} - \lim_{T \to \infty} \inf \frac{X_k(0)}{T} \ge b_0 - \lim_{T \to \infty} \inf \frac{1}{T} \sum_{t=1}^{T} b_k^{(t)}$$

$$\stackrel{(a)}{=} b_0 - \lim_{T \to \infty} \inf \frac{1}{T} \sum_{t=0}^{T-1} b_k^{(t)}$$
(37)

where (a) is due to $0 \le b_k^{(t)} \le b_{\max}$. Hence, the rate stability of $X_k(t)$ and the finiteness of $X_k(0)$ imply $\liminf_{t \ge 1} (1/T) \sum_{t=1}^{T-1} b_k^{(t)} \ge b_0$.

Based on Lemma 3, we then replace the long-term constraints (31) and (33) in \mathbf{P}_2 by rate stability constraints, leading to the following formulation with stricter constraints:

P'₂:
$$\max_{\{\mathcal{P}^{(t)}, r^{(t)}\}} \lim_{T \to \infty} \frac{1}{T} \sum_{t=0}^{T-1} r^{(t)}$$

s.t. $\{X_k(t), Y_k(t) : k \in \mathcal{K}\}$ are rate stable (1), (2), (8), (10), (13), (14), (17), (32).

B. Lyaopunov Drift Plus Penalty Method

To investigate the rate stability of all virtual queues $\{X_k(t), Y_k(t) : k \in \mathcal{K}\}$, we define the Lyapunov function [19]

$$\mathcal{L}(t) = \sum_{k=1}^{K} \frac{X_k^2(t)}{2} + \sum_{k=1}^{K} \frac{Y_k^2(t)}{2}.$$
 (38)

The Lyaopunov drift is defined as

$$\mathcal{D}(t) = \mathcal{L}(t+1) - \mathcal{L}(t). \tag{39}$$

Let $[\mathcal{P}^{(t)}]^*$ denote the policy that minimizes the Lyaopunov drift in each time slot, i.e.,

$$[\mathcal{P}^{(t)}]^* = \underset{\mathcal{P}(t)}{\arg \min} \ \mathcal{D}(t), \quad t = 0, 1, \dots$$
 (40)

Then, we have the following theorem.

Theorem 3: Let $\{X_k^*(t), Y_k^*(t) : k \in \mathcal{K}\}$ denote the virtual queues corresponding to policy $[\mathcal{P}^{(t)}]^*$ defined in (40) while $\{X_k'(t), Y_k'(t) : k \in \mathcal{K}\}$ denote the virtual queues of any other feasible policy $[\mathcal{P}^{(t)}]'$ different from $[\mathcal{P}^{(t)}]^*$. If $\{X_k'(t), Y_k'(t) : k \in \mathcal{K}\}$ are rate stable, then $\{X_k^*(t), Y_k^*(t) : k \in \mathcal{K}\}$ must be rate stable.

Theorem 3 reveals that the minimizer of $\mathcal{D}(t)$ in each time slot is more likely to achieve the rate stability of $\{X_k(t), Y_k(t) : k \in \mathcal{K}\}$ compared with any other feasible policies. In \mathbf{P}_2' , we aim to maximize $\lim_{T\to\infty} (1/T) \sum_{t=0}^{T-1} r^{(t)}$ while keeping all queues $\{X_k(t), Y_k(t) : k \in \mathcal{K}\}$ rate stable. To achieve this goal, we minimize the following drift plus penalty in each time slot [19], i.e.,

$$\min_{\mathcal{D}^{(t)}, r^{(t)}} \Phi(t) = \mathcal{D}(t) - Wr^{(t)}, \quad t = 1, 2, \dots, T$$
 (41)

where W is a positive weight to balance the two items in (41). However, minimizing $\Phi(t)$ is not easy to tackle due to the quadratic form of the Lyapunov drift $\mathcal{D}(t)$. Similarly, as in [19], we will minimize the upper bound $\bar{\Phi}(t)$ given in the following theorem instead of minimizing $\Phi(t)$ directly.

Theorem 4: $\Phi(t)$ is upper bounded by the following linear function:

$$\bar{\Phi}(t) = \sum_{k=1}^{K} \left\{ X_k(t) \left[b_0 - b_k^{(t+1)} \right] + C_0 + Y_k(t) \left[r^{(t)} - R_k^{(t)} \right] + \bar{C}_0 \right\} - W r^{(t)}$$

where $C_0 = b_{\text{max}}^2/2$ and $\bar{C}_0 = r_{\text{max}}^2/2$. *Proof:* According to (34), we have

$$X_{k}(t+1)^{2} - X_{k}(t)^{2}$$

$$= \left(\left[X_{k}(t) + b_{0} - b_{k}^{(t+1)} \right]^{+} \right)^{2} - X_{k}(t)^{2}$$

$$\leq \left[X_{k}(t) + b_{0} - b_{k}^{(t+1)} \right]^{2} - X_{k}(t)^{2}$$

$$= \left[b_{0} - b_{k}^{(t+1)} \right]^{2} + 2X_{k}(t) \left[b_{0} - b_{k}^{(t+1)} \right]$$

$$\leq b_{\max}^{2} + 2X_{k}(t) \left[b_{0} - b_{k}^{(t+1)} \right]. \tag{42}$$

From (34), we have

$$Y_{k}(t+1)^{2} - Y_{k}(t)^{2} = \left(\left[Y_{k}(t) + r^{(t)} - R_{k}^{(t)} \right]^{+} \right)^{2} - Y_{k}(t)^{2}$$

$$\leq \left[Y_{k}(t) + r^{(t)} - R_{k}^{(t)} \right]^{2} - Y_{k}(t)^{2}$$

$$= \left[r(t) - R_{k}^{(t)} \right]^{2} + 2Y_{k}(t) \left[r^{(t)} - R_{k}^{(t)} \right]$$

$$\leq r_{\max}^{2} + 2Y_{k}(t) \left[r^{(t)} - R_{k}^{(t)} \right]. \tag{43}$$

Substituting (42) and (43) into (41), we can conclude the proof.

It is noted that minimizing the upper bound $\bar{\Phi}(t)$ is also helpful to strike a balance between the objective function and the rate stability of virtual queues. For example, if $X_k(t)$ tends to rate unstable, then we have $X_k(t) \to \infty$ and $X_k(t) + b_0 - b_j^{(t+1)} \gg 0$. According to (39) and (42), we have $X_k(t)[b_0 - b_k^{(t+1)}] \to \mathcal{D}(t)$, which implies minimizing $\bar{\phi}(t)$ is equivalent to minimizing $\phi(t)$. Since the backlogs $\{X_k(t), Y_k(t): k \in \mathcal{K}\}$ are known in time slot t, minimizing $\bar{\Phi}(t)$ is equivalent to maximizing

$$\tilde{\Phi}(t) = \sum_{k=1}^{K} \left[X_k(t) b_k^{(t+1)} + Y_k(t) R_k^{(t)} \right] + \left[W - \sum_{k=1}^{K} Y_k(t) \right] r^{(t)}.$$
(44)

We can interpret the maximization of $\tilde{\Phi}(t)$ as follows. The violation of the constraint $b_k^{(t+1)} > b_0$ leads to the growth of the backlog $X_k(t)$. When $X_k(t)$ is sufficiently large to dominate $\tilde{\Phi}(t)$, maximizing $\tilde{\Phi}(t)$ is equivalent to maximizing $b_k^{(t+1)}$, which tends to satisfy $b_k^{(t+1)} > b_0$ and further reduce $X_k(t+1)$. Similarly, a large backlog $Y_k(t)$ leads to maximizing $R_k^{(t)}$ to reduce $Y_k(t+1)$.

V. OPTIMIZATION METHODS FOR EACH TIME SLOT In this section, we determine the optimal policy

$$\mathcal{P}^{(t)} = \left\{ \delta^{(t)}, \boldsymbol{\theta}^{(t)}, \boldsymbol{\eta}^{(t)}, \boldsymbol{\xi}^{(t)} \right\}$$

for each time slot t = 0, 1, 2, ..., T, by solving

$$\mathbf{P}_{3}: \max_{\mathcal{P}^{(t)}, r^{(t)}} \tilde{\Phi}(t) = \sum_{k=1}^{K} \left[X_{k}(t) b_{k}^{(t+1)} + Y_{k}(t) R_{k}^{(t)} \right] + (W - \sum_{k=1}^{K} Y_{k}(t)) r^{(t)}$$
s.t. (1), (2), (8), (10), (13), (14), (17), (32).

In \mathbf{P}_3 , $r^{(t)}$ is independent of $\mathcal{P}^{(t)}$, hence the optimal $r^{(t)}$ depends only on the backlogs $\{Y_k(t): k \in \mathcal{K}\}$, i.e.,

$$[r^{(t)}]^* = \begin{cases} r_{\text{max}}, & \text{if } \sum_{k=1}^K Y_k(t) \le W \\ 0, & \text{otherwise.} \end{cases}$$
 (45)

Next, given $\delta^{(t)}$, we set the value of $\boldsymbol{\theta}^{(t)}$, or equivalently the set of active sensors $\mathcal{K}_a^{(t)}$, in a greedy way. Specifically, we choose K_a active sensors with the largest $X_k(t)$ for $\delta^{(t)} = 1$ and choose K_a active sensors with the largest $Y_k(t)$ for $\delta^{(t)} = 0$. Then, \mathbf{P}_3 is decomposed into the following two subproblems. For $\delta^{(t)} = 1$, we aim to optimize the WPT through the downlink power control coefficients $\boldsymbol{\eta}^{(t)}$, i.e.,

$$\mathbf{P}'_3$$
: $\max_{\boldsymbol{\eta}^{(t)}} \sum_{k \in \mathcal{K}_a^{(t)}} X_k(t) b_k^{(t+1)}$
s.t. (8), (10), (17).

For $\delta^{(t)} = 0$, we aim to optimize the data transmission through the uplink power control coefficients $\boldsymbol{\xi}^{(t)}$, i.e.,

$$\mathbf{P}_{3}'': \max_{\boldsymbol{\xi}^{(t)}} \sum_{k \in \mathcal{K}_{a}^{(t)}} \left[X_{k}(t) b_{k}^{(t+1)} + Y_{k}(t) R_{k}^{(t+1)} \right]$$
s.t. (13), (14), (17),

Denote Q' and Q'' as the optimal objective values of \mathbf{P}_3' and \mathbf{P}_3'' , respectively. Then, the transmission mode $\delta^{(t)}$ is determined as

$$\left[\delta^{(t)}\right]^* = \begin{cases} 1, & \text{if } Q' \ge Q'' \\ 0, & \text{otherwise.} \end{cases}$$
 (46)

A. Solution to P_3'

Given $\delta^{(t)} = 1$, the battery state is updated according to

$$b_k^{(t+1)} = \min \Big\{ b_k^{(t)} + \tilde{\mathcal{E}}_k^{(t)}, b_{\text{max}} \Big\}.$$

Thus, \mathbf{P}_{3}' becomes

$$\max_{\boldsymbol{\eta}^{(t)}} \sum_{k \in \mathcal{K}_a^{(t)}} X_k(t) \min \left[\tilde{\mathcal{E}}_k(t), b_{\text{max}} - b_k^{(t)} \right]$$
s.t. (8), (10) (47)

which is NP-hard due to the nonconvex objective function. The difference $b_{\max} - b_k^{(t)}$ is usually much greater than $\tilde{\mathcal{E}}_k(t)$ since $b_k^{(t)}$ always fluctuates around b_0 which can be seen from the simulation results. Thus, the objective function (47) becomes

$$f(\boldsymbol{\mu}) = \sum_{k \in \mathcal{K}_{\sigma}^{(t)}} X_k(t) \tilde{\mathcal{E}}_k(t)$$
 (48)

where $\tilde{\mathcal{E}}_k(t)$ given in (25) is a function of $\mu_{l,k}^{(t)} = \sqrt{\eta_{l,k}^{(t)}} \gamma_{l,k}^{(t)}$. Using the sequential convex programming method [28], [29],

we can find a solution to (47) by sequentially maximizing the first-order approximation of $f(\mu)$

$$\widehat{f}(\boldsymbol{\mu}) = f(\widehat{\boldsymbol{\mu}}) + \sum_{l=1}^{L} \sum_{k \in \mathcal{K}_{a}^{(l)}} \frac{\partial f(\widehat{\boldsymbol{\mu}})}{\partial \widehat{\mu}_{l,k}} (\mu_{l,k} - \widehat{\mu}_{l,k})$$

near a feasible point $\widehat{\mu}$ which is updated after each iteration, i.e.,

$$\max_{\mu} \widehat{f}(\mu)$$
s.t. $\mu \in \mathcal{T}$ (49)

$$\sum_{k \in \mathcal{K}_{a}^{(t)}} \left[\mu_{l,k}^{(t)} \right]^2 / \gamma_{l,k}^{(t)} \le 1 \quad \forall l$$
(50)

where $\mathcal{T} = \{ \boldsymbol{\mu} : |\boldsymbol{\mu} - \widehat{\boldsymbol{\mu}}| \leq \rho_0 \}$ is the trust region around point $\widehat{\boldsymbol{\mu}}$, and (50) is the maximum transmit power constraint of each AP resulting from (10). After obtaining the optimal solution $\boldsymbol{\mu}^*$ of the convex problem (49), we update $\widehat{\boldsymbol{\mu}} = \boldsymbol{\mu}^*$. Until convergence, the WPT power control coefficients $\boldsymbol{\eta}^{(t)}$ is determined by $[\boldsymbol{\eta}_{l,k}^{(t)}]^* = ([\boldsymbol{\mu}_{l,k}^{(t)}]^*/\gamma_{l,k}^{(t)})^2$.

B. Solution to P_3''

Given $\delta^{(t)} = 0$, the battery state is updated according to

$$b_k^{(t+1)} = b_k^{(t)} - (1 - \alpha)\rho_u \theta_i^{(t)} \xi_i^{(t)}.$$

Hence, P_3'' can be rewritten as

$$\max_{\boldsymbol{\xi}^{(t)}} \sum_{k \in \mathcal{K}_a^{(t)}} \left[Y_k(t) R_k^{(t)} - (1 - \alpha) X_k(t) \rho_u \boldsymbol{\xi}_k^{(t)} \right]$$
s.t. (13), (14) (51)

which aim to strike a balance between the weighted sum rate and the weighted transmit power consumption. Solving (51) is equivalent to solving a series of subproblems for fixed

$$\sum_{k \in \mathcal{K}_{\alpha}^{(t)}} (1 - \alpha) X_k(t) \rho_u \xi_k^{(t)} = \chi$$

with $\chi \in (0, (1 - \alpha) \sum_{k \in \mathcal{K}_a^{(t)}} X_k(t) \rho_u)$. According to (15) and (27), subproblems can be written as

$$\max_{\xi^{(t)}} \sum_{k \in \mathcal{K}_a^{(t)}} (1 - \alpha) Y_k(t) \log_2 \left(1 + \frac{A_k^{(t)}}{B_k^{(t)}} \right)$$
 (52)

s.t.
$$\sum_{k \in \mathcal{K}_a^{(t)}} (1 - \alpha) X_k(t) \rho_u \xi_k^{(t)} = \chi$$
(13), (14) (53)

where

$$A_k^{(t)} = \mathcal{D}_k^{(t)} \xi_k^{(t)}$$

and

$$B_k^{(t)} = \mathcal{U}_k^{(t)} \xi_k^{(t)} + \sum_{i \in \mathcal{K}_{o}^{(t)}/\{k\}} \mathcal{I}_{k,j}^{(t)} \xi_j^{(t)} + \mathcal{N}_k^{(t)}$$

Algorithm 1 Proposed Long-Term Scheduling and Power Control Algorithm

- 1: **Input**: The large-scale fading coefficients $\{\beta_{l,k}, l = 1, \ldots, L, k \in \mathcal{K}\}$.
- 2: **Initialization**: Set T_{max} and initialize the backlogs $\{X_k(0) = Y_k(0) = 0 : k \in \mathcal{K}\}.$
- 3: **for** $t = 1 : T_{\text{max}}$ **do**
- 4: According to the current backlogs $\{Y_k(t): k \in \mathcal{K}\}$, obtain the optimal auxiliary variables $[r^{(t)}]^*$ according to (45).
- 5: Solve problem \mathbf{P}'_3 according to Section V-A, obtain the optimal solution $[\boldsymbol{\eta}^{(t)}]^*$ and the corresponding objective value O'.
- 6: Solve problem \mathbf{P}_3'' according to Section V-B, obtain the optimal solution $[\boldsymbol{\xi}^{(t)}]^*$ and the corresponding objective value Q''.
- 7: Determine the optimal transmission mode $[\delta^{(t)}]^*$ and the corresponding sensor states $[\theta^{(t)}]^*$ according to (46). and select the optimal corresponding power control coefficients.
- 8: Update the virtual queues $\{X_k(t+1), Y_k(t+1) : k \in \mathcal{K}\}$ using the optimal $[\mathcal{P}^{(t)}]^*$ according to (34) and (35).
- 9: end for
- 10: **Output**: The policy for each time slot $[\mathcal{P}^{(t)}]^*$.

which implies (52) is a standard weighted sum-of-logarithms maximization problem [30]–[32]. Introducing the auxiliary variables $\{\omega_k, k \in \mathcal{K}_a^{(t)}\}$, (52) is equivalent to

$$\max_{\boldsymbol{\xi}^{(t)}, \{\omega_k\}} \sum_{k \in \mathcal{K}_a^{(t)}} (1 - \alpha) Y_k(t) \left[\log_2(1 + \omega_k) - \omega_k \right] + \sum_{k \in \mathcal{K}_a^{(t)}} \frac{(1 - \alpha) Y_k(t) (1 + \omega_k) A_k^{(t)}}{A_k^{(t)} + B_k^{(t)}}$$
s.t. (13), (14), (53) (54)

which has been proved in [32]. Then, we alternately solve $\boldsymbol{\xi}^{(t)}$ and $\{\omega_k\}$ while fixing the other. For fixed $\boldsymbol{\xi}^{(t)}$, the optimal $\{\omega_k\}$ is given by $\omega_k^* = \Gamma_k^{(t)}$ using the KKT condition. For fixed $\{\omega_k\}$, (54) is reduced to a sum-of-ratios maximization problem which can be solved using the quadratic transform-based fractional optimization technique proposed in [31] and [32].

C. Overall Algorithm

Finally, the proposed long-term scheduling and power control algorithm for solving \mathbf{P}_1 in (20) is summarized in Algorithm 1.

VI. SIMULATION RESULTS

In this section, simulation results are provided to verify the accuracy of closed-form expressions and the performance of our proposed scheduling and power control approach.

A. Simulation Setup

We consider a large square hall of $50 \times 50 \text{ m}^2$ with wrapped around to avoid boundary effects. L = 100 APs are placed

TABLE I SIMULATION PARAMETERS

parameter	Meaning	Value
L	Number of APs	100
N	Number of antennas of each AP	10
K	Number of all sensors	200
В	Bandwidth	20 MHz
Δ/T_c	Coherence time	0.2 s/200 symbols
τ	Length of pilot	60 symbols
ρ_p	Pilot transmit power	0.2 mW
ρ_u	Maximum uplink transmit power	20 mW
ζ	Energy conversion efficiency	1
$ ho_d$	Maximum downlink transmit power	20 W
$\delta^{(t)}$	Transmission model	Optimized
$oldsymbol{ heta}^{(t)}$	Active sensor set	Optimized
$oldsymbol{\eta}^{(t)}$	Downlink power control coefficients	Optimized
$\boldsymbol{\xi}^{(t)}$	Uplink power control coefficients	Optimized
$b_{ m max}$	Capacity of the battery	300mJ
b_0	Predefined threshold	$10 \ mJ$

on $h_{\rm AP}=7$ m high ceiling to form a uniform square array. K=200 sensors with height $h_{\rm s}=1.65$ m are randomly distributed in this area. We model the large-scale fading $\beta_{l,k}$ as

$$\beta_{l,k} = \mathcal{L}_{l,k} 10^{\frac{\sigma_{sh}z_{l,k}}{10}}$$

where $10^{([\sigma_{sh}z_{l,k}]/10)}$ denotes the shadow fading with $\sigma_{sh} = 8$ dB and $z_{l,k} \sim \mathcal{CN}(0,1)$, and the path loss $\mathcal{L}_{l,k}$ (dB) is given by

$$\mathcal{L}_{l,k} = \begin{cases} -\mathcal{L}_0 - 35\log_{10}(d_{l,k}), & \text{if } d_{l,k} > d_1 \\ -\mathcal{L}_0 - 15\log_{10}(d_1) - 20\log_{10}(d_{l,k}), & \text{if } d_0 < d_{l,k} \le d_1 \\ -\mathcal{L}_0 - 15\log_{10}(d_1) - 20\log_{10}(d_0), & \text{if } d_{l,k} \le d_0 \end{cases}$$

where $d_0 = 10 \text{ m}, d_1 = 50 \text{ m}, \text{ and}$

$$\mathcal{L}_0 \triangleq 46.3 + 33.9 \log_{10}(f) - 13.82 \log_{10}(h_{AP}) - (1.1 \log_{10}(f) - 0.7)h_s + (1.56 \log_{10}(f) - 0.8)$$

with carrier frequency f = 1900 MHz. The noise power is

$$\sigma^2 = B \times k_B \times T_0 \times \kappa$$

where $k_B = 1.381 \times 10^{-23}$ J/K, $T_0 = 290$ K, $\kappa = 9$ dB, and the bandwidth B = 20 MHz. The other simulation parameters are summarized in Table I. In addition, the large-scale fading $\{\beta_{l,k} \ \forall l, k\}$ are generated once and fixed for all simulations.

B. Accuracy of Expressions

Through a realization with $K_a = 30$ sensors randomly scheduled, the accuracy of the closed-form expressions $\bar{\mathcal{E}}_k^{(t)}$ in (26) and $\bar{R}_k^{(t)}$ in (28) are verified in Figs. 2 and 3, respectively. In Fig. 2, the closed-form expressions $\bar{\mathcal{E}}_k$ independent of random pilots are compared with the simulation results obtained through 500 realizations of random pilot sequences with the uniform power control, i.e., $\eta_{l,k}^{(t)} \gamma_{l,k}^{(t)} = 1/K_a \ \forall l$, and $k \in \mathcal{K}_a^{(t)}$. The figure shows that the closed-form expressions agree well with the mean of simulation results. In addition, the small variances of simulation results stemming

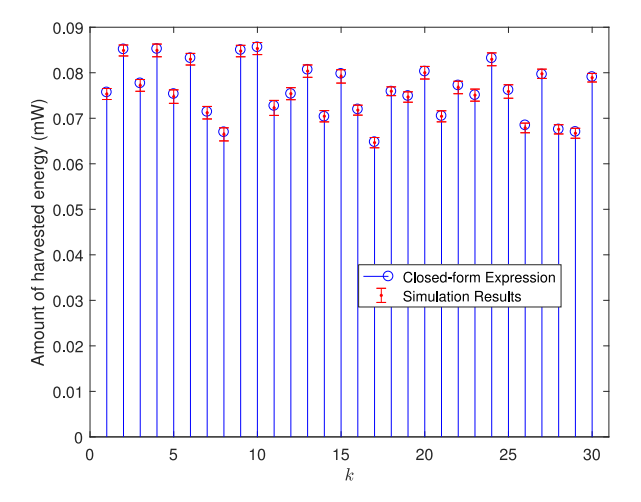


Fig. 2. Accuracy of the amount of harvested energy $\bar{\mathcal{E}}_{k}^{(t)}$ given in (26).

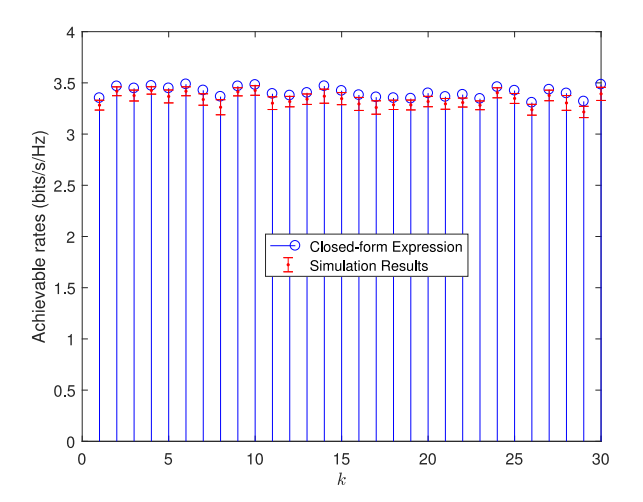


Fig. 3. Accuracy of the achievable rate $\bar{R}_{k}^{(t)}$ given in (28).

from random pilots reveal that pilot optimization over random pilots is not necessary.

In Fig. 3, the closed-form expressions $\bar{R}_k^{(t)}$ independent of random pilots are compared with the simulation results obtained through 500 realizations of random pilot sequences with uniform power control, i.e., $\xi_k^{(t)} = 1, k \in \mathcal{K}_a^{(t)}$. Similarly, as in Fig. 2, it can be seen that the difference between the closed-form expressions and the simulation results is small.

To investigate the impact of enlarging the active set $\mathcal{K}_a^{(t)}$, the average $\bar{\mathcal{E}}_k^{(t)}$ and $\bar{R}_k^{(t)}$ obtained through 500 random schedule realizations versus K_a is plotted in Fig. 4. As noted in Remark 1, the metrics $\bar{\mathcal{E}}_k^{(t)}$ and $\bar{R}_k^{(t)}$ decrease as K_a increases. In addition, it can be seen that $\bar{\mathcal{E}}_k^{(t)}$ is more sensitive to K_a , which implies the importance of scheduling during WPT.

C. Performance Comparison

In this section, we evaluate the performance of our proposed long-term scheduling and power control approach. To the best of our knowledge, there is no existing work to investigate the long-term scheduling and power control scheme for a wirelessly powered cell-free IoT network. For comparison, we consider the following simple greedy scheme as a

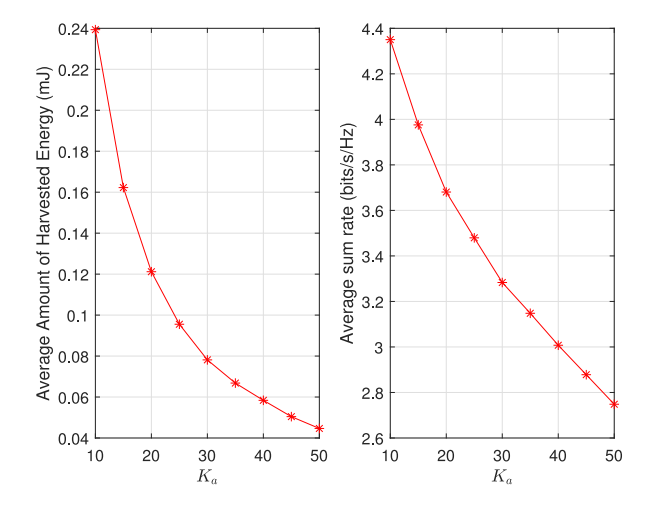


Fig. 4. Average amount of harvested energy and average achievable rate versus the number of scheduled sensors $K_a^{(t)}$.

benchmark. In each time slot for transmission mode, K_a sensors with the largest $b_k^{(t)}$ are scheduled for data transmission with $\xi_k^{(t)}=1, k\in\mathcal{K}_a^{(t)}$. The transmission mode continues until there exits some sensors whose battery is depleted, i.e., $b_k^{(t)}=0$, and then the harvesting mode is triggered. In each time slot for harvesting, K_a sensors with the lowest $b_k^{(t)}$ are scheduled for WPT with the uniform power allocation, i.e., $\eta_{l,k}^{(t)}\gamma_{l,k}^{(t)}=1/K_a~\forall l,~$ and $k\in\mathcal{K}_a^{(t)}$. Until $b_k^{(t)}\geq b_0, k\in\mathcal{K}$, the transmission mode is triggered again. In our simulations, we consider $K_a=30$ and 100.

Figs. 5 and 6 plot the dynamic of the minimum time-average rate with $K_a = 30$ and 100, respectively. It can be seen that the minimum time-average rate becomes stable after about 1000 time slots. The shadowed error bar is

$$\hat{\sigma}^{(T)} = \sqrt{\frac{\sum_{k=1}^{K} \left[\frac{1}{T} \sum_{t=0}^{T-1} R_k^{(t)} - \overline{R^{(T)}}\right]^2}{K}}$$

where $\overline{R^{(T)}} = \{(1/T)\sum_{t=0}^{T-1}\sum_{k=1}^K R_k^{(t)}\}/K$ is the mean of time-average rates over all sensors. The small shadowed error bar reflects the max-min fairness of our proposed approach. Compared with the greedy benchmark, our proposed approach can boost the minimum time-average rate significantly. The improvement mainly results from two aspects. On the one hand, the power consumption for data transmission is significantly reduced since (51) strikes a balance between the spectrum efficiency and the power consumption, instead of focusing only on the spectrum efficiency. On the other hand, the WPT efficiency is improved by optimizing the downlink power control coefficients and scheduling. Moreover, it is seen that a larger W leads to a higher minimum time-average rate and requires more time slots to achieve the rate stability. Comparing Figs. 5 and 6, the minimum time-average rate becomes smaller as K_a increased from 30 to 100 although more sensors are active in each time slot. This is because the accuracy of channel estimation is reduced by enlarging the active set $\mathcal{K}_a^{(t)}$, which is noted in Remark 1.

To investigate the rate stability of the virtual queues, Fig. 7 shows the sum of time-average backlogs $\overline{X}(t)$ and $\overline{Y}(t)$ versus

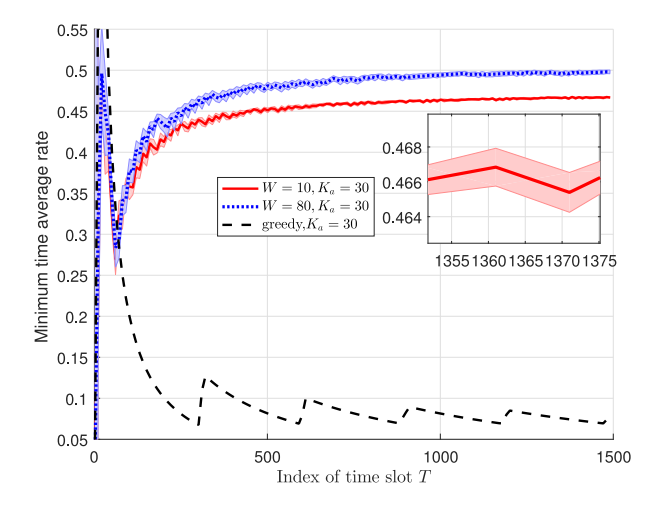


Fig. 5. Minimum time average rate versus the index of time slot with $K_a = 30$.

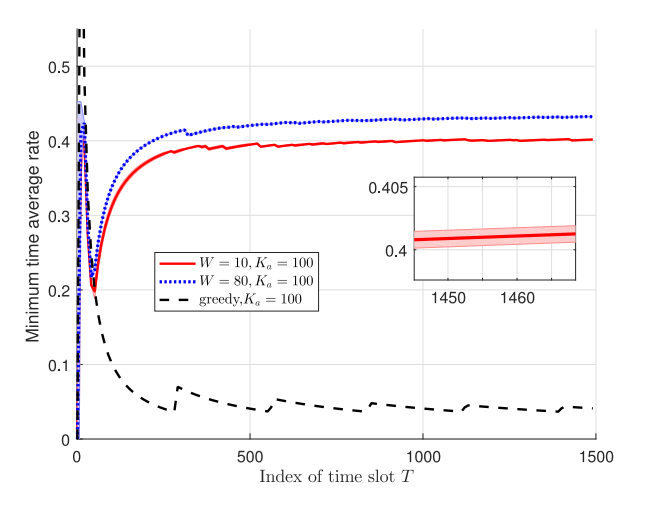


Fig. 6. Minimum time average rate versus the index of time slot with $K_a = 100$.

the index of time slot with different W, where

$$\overline{X}(t) = \frac{1}{T} \sum_{t=0}^{T-1} \sum_{k=1}^{K} X_k(t)$$
, and $\overline{Y}(t) = \frac{1}{T} \sum_{t=0}^{T-1} \sum_{k=1}^{K} Y_k(t)$.

The nonincreasing $\overline{X}(t)$ and $\overline{Y}(t)$ reveal that $\{X_k(t), Y_k(t) : k \in \mathcal{K}\}$ are rate stable, which implies the long-term constraints (31) and (33) of problem \mathbf{P}_2 are satisfied. With the increase of W, the time-average backlogs $\overline{X}(t)$ and $\overline{Y}(t)$ also increase. Fig. 8 plots the dynamic of the battery state $\{b_k^{(t)} : k \in \mathcal{K}\}$ versus the index of time slot. It can be seen $b_k^{(t)}$ always fluctuates across the predefined b_0 , which implies that the batteries are never exhausted. If $b_k^{(t)}$ is smaller than b_0 for some continuous time slots, the corresponding backlog $X_k(t)$ would increase continuously, and then trigger power transfer to increase $b_k^{(t)}$ and avoid the depletion of the battery.

VII. CONCLUSION

In this article, we have considered the long-term scheduling and power control in a wirelessly powered cell-free IoT network. We first derived closed-form expressions for the harvested energy and the achievable rates, and then formulated a

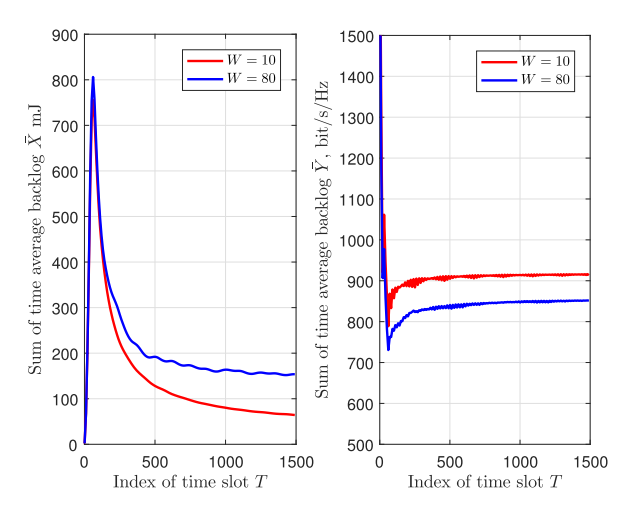


Fig. 7. Backlogs versus the index of time slot with different W.

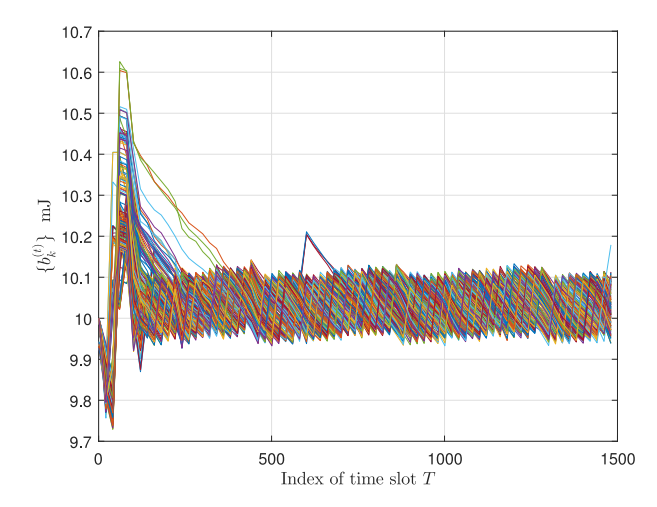


Fig. 8. Dynamic of $\{b_k^{(t)}: k \in \mathcal{K}\}\$ with W = 10.

long-term scheduling and power control problem to maximize the minimum time-average achievable rate. Following the Lyapunov optimization approach, the transmission mode, the sensor state, and the uplink and downlink power control coefficients are jointly determined for each time slot. The simulation results reveal that the proposed long-term scheduling and power control approach can boost the max—min time-average achievable rate significantly.

APPENDIX A PROOF OF THEOREM 1

To prove Theorem 1, we first introduce the following two lemmas.

Lemma 5 [26]: Let $A \in \mathbb{C}^{\tau \times \tau}$ is a Hermitian invertible matrix. Then, for any vector $\mathbf{x} \in \mathbb{C}^{\tau}$ and any scalar $a \in \mathbb{C}$ such that $A + a\mathbf{x}\mathbf{x}^H$ is invertible

$$x^{H} (A + axx^{H})^{-1} = \frac{x^{H} A^{-1}}{1 + ax^{H} A^{-1} x}.$$
 (55)

Lemma 6 [26]: Let $A \in \mathbb{C}^{\tau \times \tau}$, and $x, y \sim \mathcal{CN}(\mathbf{0}, [1/\tau]I_{\tau})$. Assume that A has uniformly bounded spectral norm (w.r.t. τ) and that x and y are mutually independent and independent of

A, we have

$$x^H A x - \text{tr} A / \tau \xrightarrow{\text{a.s.}} 0$$
 (56)

$$x^H A y \xrightarrow{\text{a.s.}} 0.$$
 (57)

Substituting $\mathbf{Z}_{l,k}^{(t)} = \mathbf{Z}_{l}^{(t)} - E_{p}\beta_{l,k}\boldsymbol{\psi}_{k}\boldsymbol{\psi}_{k}^{H}$ into (6), and using (55), we obtain

$$\gamma_{l,k}^{(t)} = E_p \beta_{l,k}^2 \boldsymbol{\psi}_k^H \left(\mathbf{Z}_{l,k}^{(t)} + E_p \beta_{l,k} \boldsymbol{\psi}_k \boldsymbol{\psi}_k^H \right)^{-1} \boldsymbol{\psi}_k$$

$$= \frac{E_p \beta_{l,k}^2 \boldsymbol{\psi}_k^H \left(\mathbf{Z}_{l,k}^{(t)} \right)^{-1} \boldsymbol{\psi}_k}{1 + E_p \beta_{l,k} \boldsymbol{\psi}_k^H \left(\mathbf{Z}_{l,k}^{(t)} \right)^{-1} \boldsymbol{\psi}_k}.$$

Since $\psi_k \sim \mathcal{CN}(0, [1/\tau]I)$ is independent of $[\mathbf{Z}_{l,k}^{(t)}]^{-1}$, using (56), we have

$$\gamma_{l,k}^{(t)} - \frac{E_p \beta_{l,k}^2 \text{tr} \left[\left(\mathbf{Z}_{l,k}^{(t)} \right)^{-1} \right] / \tau}{1 + E_p \beta_{l,k} \text{tr} \left[\left(\mathbf{Z}_{l,k}^{(t)} \right)^{-1} \right] / \tau} \xrightarrow{\text{a.s.}} 0$$
 (58)

Substituting (21) into (58), we conclude the proof.

APPENDIX B PROOF OF THEOREM 2

Since $\boldsymbol{a}_{l,k}^{(t)} = \sqrt{E_p} \beta_{l,k} [\boldsymbol{Z}_l^{(t)}]^{-1} \boldsymbol{\psi}_k$, using (55)–(57), we obtain

$$\left\|\boldsymbol{a}_{l,k}^{(t)}\right\|^{2} - \frac{E_{p}\beta_{l,k}^{2} \operatorname{tr}\left\{\left[\boldsymbol{Z}_{l,k}^{(t)}\right]^{-2}\right\}/\tau}{\left(1 + E_{p}\beta_{l,k} \operatorname{tr}\left\{\left[\boldsymbol{Z}_{l,k}^{(t)}\right]^{-1}\right\}/\tau\right)^{2}} \xrightarrow{\text{a.s.}} 0 \quad (59)$$

$$\boldsymbol{\psi}_{k}^{H}\boldsymbol{a}_{l,k}^{(t)} - \frac{\sqrt{E_{p}}\beta_{l,k} \operatorname{tr}\left\{\left[\boldsymbol{Z}_{l,k}^{(t)}\right]^{-1}\right\}/\tau}{1 + E_{p}\beta_{l,k} \operatorname{tr}\left\{\left[\boldsymbol{Z}_{l,k}^{(t)}\right]^{-1}\right\}/\tau} \xrightarrow{\text{a.s.}} 0$$
 (60)

and

$$\boldsymbol{\psi}_{i}^{H}\boldsymbol{a}_{l,k}^{(t)} \stackrel{\text{a.s.}}{\longrightarrow} 0, \quad (i \neq k). \tag{61}$$

Substituting (21)–(23) and (59)–(61) into (27), we can conclude the proof.

APPENDIX C PROOF OF LEMMA 3

According to (30) and (58), we have

$$\bar{e}_{l,k}^{(t)} - \frac{\beta_{l,k}}{1 + E_p \beta_{l,k} \text{tr} \left[\left(\mathbf{Z}_{l,k}^{(t)} \right)^{-1} \right] / \tau} \xrightarrow{\text{a.s.}} 0$$
 (62)

$$\left[\bar{e}_{l,k}^{(t)}\right]' - \frac{\beta_{l,k}}{1 + E_p \beta_{l,k} \text{tr} \left\{ \left[\left(\mathbf{Z}_{l,k}^{(t)} \right)' \right]^{-1} \right\} / \tau} \xrightarrow{\text{a.s.}} 0. \quad (63)$$

Without loss of generality, we assume

$$\left[\mathbf{Z}_{l,k}^{(t)}\right]' = \mathbf{Z}_{l,k}^{(t)} + E_p \beta_j \boldsymbol{\psi}_{l,j} \boldsymbol{\psi}_j^H, j \in \left[\mathcal{K}_a^{(t)}\right]', j \notin \mathcal{K}_a^{(t)}.$$

Using (55), we have

$$\operatorname{tr}\left\{\left[\left(\mathbf{Z}_{l,k}^{(t)}\right)'\right]^{-1}\right\} = \operatorname{tr}\left\{\left[\mathbf{Z}_{l,k}^{(t)}\right]^{-1}\right\} - \frac{E_{p}\beta_{l,j}\boldsymbol{\psi}_{j}^{H}\left[\mathbf{Z}_{l,k}^{(t)}\right]^{-2}\boldsymbol{\psi}_{j}}{1 + E_{p}\beta_{l,j}\boldsymbol{\psi}_{j}^{H}\left[\mathbf{Z}_{l,k}^{(t)}\right]^{-1}\boldsymbol{\psi}_{j}}$$

$$\stackrel{\text{a.s.}}{\longrightarrow} \operatorname{tr}\left\{\left[\mathbf{Z}_{l,k}^{(t)}\right]^{-1}\right\} - \frac{E_{p}\beta_{l,j}\operatorname{tr}\left\{\left[\mathbf{Z}_{l,k}^{(t)}\right]^{-2}\right\}}{1 + E_{p}\beta_{l,j}\operatorname{tr}\left\{\left[\mathbf{Z}_{l,k}^{(t)}\right]^{-1}\right\}}$$

$$< \operatorname{tr}\left\{\left[\mathbf{Z}_{l,k}^{(t)}\right]^{-1}\right\}$$

$$(64)$$

where the second step follows from (56) due to the independence of ψ_j and $[\mathbf{Z}_{l,k}^{(t)}]^{-1}$. Substituting (64) into (62) and (63), we can conclude the proof.

APPENDIX D

PROOF OF THEOREM 3

According to the definition $[\mathcal{P}^{(t)}]^*$ in (40), we have

$$\mathcal{D}^*(t) \le \mathcal{D}'(t) \tag{65}$$

in each time slot t=0,1,... From the identical initial point $X_k^*(0)=X_k'(0)=X_k(0), Y_k^*(0)=Y_k'(0)=Y_k(0), k=1,...,K$, using (39) and (65), we can obtain

$$\mathcal{L}'(1) = \mathcal{D}'(0) + \sum_{k=1}^{K} \left\{ \left[X_k'(0) \right]^2 + \left[Y_k'(0) \right]^2 \right\}$$

$$\geq \mathcal{D}^*(0) + \sum_{k=1}^{K} \left\{ \left[X_k(0) \right]^2 + \left[Y_k(0) \right]^2 \right\} = \mathcal{L}^*(1) \quad (66)$$

where $\mathcal{L}'(t) = \sum_{k=1}^{K} \{ [X_k'(t)]^2 + [Y_k'(t)]^2 \}$ and $\mathcal{L}^*(t) = \sum_{k=1}^{K} \{ [X_k^*(t)]^2 + [Y_k^*(t)]^2 \}$. For any given time slot t with $\mathcal{L}^*(t) \leq \mathcal{L}'(t)$, using (39) and (65), we have

$$\mathcal{L}^{*}(t+1) - \mathcal{L}^{*}(t) \leq \mathcal{L}'(t+1) - \mathcal{L}'(t)$$

$$= \sum_{k=1}^{K} \left\{ \left[X'_{k}(t+1) \right]^{2} + \left[Y'_{k}(t+1) \right]^{2} \right\}$$

$$- \sum_{k=1}^{K} \left\{ \left[X'_{k}(t) \right]^{2} + \left[Y'_{k}(t) \right]^{2} \right\}$$

$$\leq \mathcal{L}'(t+1) - \mathcal{L}^{*}(t)$$

which implies

$$\mathcal{L}^*(t+1) \le \mathcal{L}'(t+1). \tag{67}$$

From (66) and (67), we can conclude that

$$\sum_{k=1}^{K} \left\{ \left[X_k^*(T) \right]^2 + \left[Y_k^*(T) \right]^2 \right\} \le \sum_{k=1}^{K} \left\{ \left[X_k'(T) \right]^2 + \left[Y_k'(T) \right]^2 \right\}$$
(68)

for any given T. When $\{X_k'(t), Y_k'(t) : k = 1, ..., K, \}$ are rate stable, (68) is equivalent to

$$\lim_{T \to \infty} \frac{1}{T} \sum_{k=1}^{K} \left\{ \left[X_k^*(T) \right]^2 + \left[Y_k^*(T) \right]^2 \right\} \le 0 \tag{69}$$

which implies $\{X_k^*(t), Y_k^*(t) : k = 1, ..., K, \}$ are rate stable. Then, we conclude the proof.

REFERENCES

[1] A. Al-Fuqaha, M. Guizani, M. Mohammadi, M. Aledhari, and M. Ayyash, "Internet of Things: A survey on enabling technologies, protocols, and applications," *IEEE Commun. Surveys Tuts.*, vol. 17, no. 4, pp. 2347–2376, 4th Quart., 2015. [2] F. Javed, M. K. Afzal, M. Sharif, and B. Kim, "Internet of Things

(IoT) operating systems support, networking technologies, applications, and challenges: A comparative review," *IEEE Commun. Surveys Tuts.*, vol. 20, no. 3, pp. 2062–2100, 3rd Quart., 2018.

[3] Z. Chu, F. Zhou, Z. Zhu, R. Q. Hu, and P. Xiao, "Wireless powered sen-

sor networks for Internet of Things: Maximum throughput and optimal power allocation," *IEEE Internet Things J.*, vol. 5, no. 1, pp. 310–321,

- [4] Y. Xiao, M. Krunz, and T. Shu, "Multi-operator network sharing for massive IoT," IEEE Commun. Mag., vol. 57, no. 4, pp. 96–101, Apr. 2019.
- K. Mikhaylov et al., "Energy efficiency of multi-radio massive machine-type communication (MR-MMTC): Applications, challenges, and solu-tions," *IEEE Commun. Mag.*, vol. 57, no. 6, pp. 100–106, Jun. 2019. L. Liu, R. Zhang, and K.-C. Chua, "Multi-antenna wireless pow-
- ered communication with energy beamforming," *IEEE Trans. Commun.*, vol. 62, no. 12, pp. 4349–4361, Dec. 2014.
- S. Kashyap, E. Björnson, and E. G. Larsson, "On the feasibility of wireless energy transfer using massive antenna arrays," *IEEE Trans.*
- Wireless Commun., vol. 15, no. 5, pp. 3466–3480, May 2016.

 T. D. Ponnimbaduge Perera, D. N. K. Jayakody, S. K. Sharma, S. Chatzinotas, and J. Li, "Simultaneous wireless information and power transfer (SWIPT): Recent advances and future challenges," IEEE Commun. Surveys Tuts., vol. 20, no. 1, pp. 264–302, 1st Quart., 2018. J. Huang, C. Xing, and C. Wang, "Simultaneous wireless information
- and power transfer: Technologies, applications, and research challenges," *IEEE Commun. Mag.*, vol. 55, no. 11, pp. 26–32, Nov. 2017.

 [10] S. Bi and R. Zhang, "Placement optimization of energy and information
- access points in wireless powered communication networks," *IEE Trans. Wireless Commun.*, vol. 15, no. 3, pp. 2351–2364, Mar. 2016.
- [11] J. Chen, L. Zhang, Y. Liang, X. Kang, and R. Zhang, "Resource allocation for wireless-powered IoT networks with short packet communication," *IEEE Trans. Wireless Commun.*, vol. 18, no. 2, pp. 1447–1461,
- [12] T. A. Khan, A. Yazdan, and R. W. Heath, "Optimization of power transfer efficiency and energy efficiency for wireless-powered systems with massive MIMO," IEEE Trans. Wireless Commun., vol. 17, no. 11, op. 7159–7172, Nov. 2018.
- [13] H. Q. Ngo, A. Ashikhmin, H. Yang, E. G. Larsson, and T. L. Marzetta, 'Cell-free massive MIMO versus small cells," IEEE Trans. Wireless
- "Cell-tree massive MIMO versus small cells," *IEEE Trans. Wireless Commun.*, vol. 16, no. 3, pp. 1834–1850, Mar. 2017.
 [14] E. Nayebi, A. Ashikhmin, T. L. Marzetta, H. Yang, and B. D. Rao, "Precoding and power optimization in cell-free massive MIMO systems," *IEEE Trans. Wireless Commun.*, vol. 16, no. 7, pp. 4445–4459, Jul. 2017.
 [15] X. Wang, A. Ashikhmin, and X. Wang, "Wirelessly powered cell-free IoT: Analysis and optimization," *IEEE Internet Things J.*, early access, Apr. 27, 2020, doi: 10.1109/JIOT.2020.2990378.
 [16] S. Rao, A. Ashikhmin, and H. Yang, "Internet of Things based on
- [16] S. Rao, A. Ashikhmin, and H. Yang, "Internet of Things based on cell-free massive MIMO," in *Proc. 53rd Asilomar Conf. Signals Syst. Comput.*, Pacific Grove, CA, USA, 2019, pp. 1946–1950.
 [17] M. Mollanoori and M. Ghaderi, "Uplink scheduling in wireless networks
- with successive interference cancellation," *IEEE Trans. Mobile Comput.*, vol. 13, no. 5, pp. 1132–1144, May 2014.

 X. Wang and L. Cai, "Proportional fair scheduling in hierarchical modulation aided wireless networks," *IEEE Trans. Wireless Commun.*, vol. 12,
- no. 4, pp. 1584–1593, Apr. 2013. [19] M. J. Neely, "Stochastic network optimization with application to communication and queueing systems," in Synthesis Lectures on Communication Networks, vol. 3. San Rafael, CA, USA: Morgan & Claypool, 2010, pp. 1-211.
- [20] S. Pan and Y. Chen, "Energy-optimal scheduling of mobile cloud computing based on a modified Lyapunov optimization method," IEEE Frans. Green Commun. Netw., vol. 3, no. 1, pp. 227–235, Mar. 2019.
- [21] D. Zhai, R. Zhang, L. Cai, B. Li, and Y. Jiang, "Energy-efficient user scheduling and power allocation for NOMA-based wireless networks with massive IoT devices," IEEE Internet Things J., vol. 5, no. 3, pp. 1857–1868, Jun. 2018.
- [22] K. Choi and D. Kim, "Stochastic optimal control for wireless powered communication networks," IEEE Trans. Wireless Commun., vol. 15, no. 1, pp. 686-698, Jan. 2016.
- [23] W. Ma, W. Wang, and T. Jiang, "Energy beamforming for wireless information and power transfer in backscatter multiuser networks," in Proc. IEEE Global Commun. Conf. (GLOBECOM), Waikoloa, HI, USA,
- 2019, pp. 1–6. G. Song, W. Wang, D. Chen, and T. Jiang, "KPI/KQI-driven coordinated multipoint in 5G: Measurements, field trials, and technical solutions,"
- IEEE Wireless Commun., vol. 25, no. 5, pp. 23–29, Oct. 2018.

 [25] M. Peng, Y. Yu, H. Xiang, and H. V. Poor, "Energy-efficient resource allocation optimization for multiallocation optimization for multimedia heterogeneous cloud radio access networks," IEEE Trans. Multimedia, vol. 18, no. 5, pp. 879-892, May 2016.

- [26] J. Hoydis, S. Ten Brink, and M. Debbah, "Massive MIMO in the UL/DL of cellular networks: How many antennas do we need?" IEEE J. Sel. Areas Commun., vol. 31, no. 2, pp. 160-171, Feb. 2013.
- [27] Z. Jing, Q. Yang, M. Qin, and K. S. Kwak, "Long term max-min fairness guarantee mechanism: Adaptive task splitting and resource allocation in MEC-enabled networks," in *Proc. IEEE 30th Int. Symp. Pers. Indoor Mobile Radio Commun. (PIMRC Workshop)*, Istanbul, Turkey, 2019,
- pp. 1-6. T. Lipp and S. Boyd, "Variations and extension of the convex-concave
- procedure," *Optim. Eng.*, vol. 17, no. 2, pp. 263–287, 2016. S. K. Joshi, K. B. S. Manosha, M. Codreanu, and M. Latva-Aho, "Dynamic inter-operator spectrum sharing via Lyapunov optimization, IEEE Trans. Wireless Commun., vol. 16, no. 10, pp. 6365-6381, Oct. 2017.
- [30] H. Guo, Y.-C. Liang, J. Chen, and E. G. Larsson, "Weighted sum-rate maximization for reconfigurable intelligent surface aided wireless networks," IEEE Trans. Wireless Commun., vol. 19, no. 5,
- pp. 3064–3076, May 2020.

 [31] K. Shen and W. Yu, "Fractional programming for communication systems—Part I: Power control and beamforming," *IEEE Trans. Signal*
- Process., vol. 66, no. 10, pp. 2616–2630, May 2018.

 [32] K. Shen and W. Yu, "Fractional programming for communication systems—Part II: Uplink scheduling via matching," *IEEE Trans. Signal Process.*, vol. 66, no. 10, pp. 2631–2644, May 2018.



Xinhua Wang (Member, IEEE) received the Ph.D. degree in communication and information system from Shandong University, Jinan, China, in 2016.

In June 2016, he joined the College of Electrical Engineering, Qingdao University, Qingdao, China, as a Lecturer. His research interests include massive MIMO, cell-free massive MIMO, compressed sensing, and random matrix theory.



Xiaodong Wang (Fellow, IEEE) received the Ph.D. degree in electrical engineering from Princeton University, Princeton, NJ, USA, in 1998.

He is a Professor of electrical engineering with Columbia University, New York, NY, USA. His research interests fall in the general areas of computing, signal processing, and communications, and has published extensively in these areas. Among his publications is a book titled Wireless Communication Systems: Advanced Techniques for Signal Reception (Prentice-Hall, 2003). His current research interests

include wireless communications, statistical signal processing, and genomic signal processing.

Prof. Wang received the 1999 NSF CAREER Award, the 2001 IEEE Communications Society and Information Theory Society Joint Paper Award, and the 2011 IEEE Communication Society Award for Outstanding Paper on New Communication Topics. He has served as an Associate Editor for the IEEE TRANSACTIONS ON COMMUNICATIONS, the IEEE TRANSACTIONS ON WIRELESS COMMUNICATIONS, the IEEE TRANSACTIONS ON SIGNAL PROCESSING, and the IEEE TRANSACTIONS ON INFORMATION THEORY. He is listed as an ISI Highly Cited Author.



Alexei Ashikhmin (Fellow, IEEE) received the Ph.D. degree in electrical engineering from the Institute of Information Transmission Problems, Russian Academy of Science, Moscow, Russia, in 1994

He is a Distinguished Member of Technical Staff with the Mathematics and Algorithms of Communications Department, Nokia Bell Labs, Murray Hill, NJ, USA. He is also an Adjunct Professor with Columbia University, New York, NY, USA, where he teaches courses on quantum com-

puting and error correction, digital communications, and error correcting codes. His research interests include communications theory, massive MIMO systems, theory of error correcting codes and its modern applications, as well as classical and quantum information theory

Dr. Ashikhmin was a recipient of the 2017 SPS Donald G. Fink Overview Paper Award for the article "An Overview of Massive MIMO: Benefits and Challenges" published in the IEEE JOURNAL OF SELECTED TOPICS IN SIGNAL PROCESSING. In 2014, he received the Thomas Edison Patent Award in the Telecommunications for a Patent on Massive MIMO System with Decentralized Service Antennas. In 2004, he received the IEEE Communications Society Stephen O. Rice Prize for the best paper published in IEEE TRANSACTIONS ON COMMUNICATIONS. In 2002, 2010, and 2011, he was a recipient of the Bell Laboratories President Award for breakthrough research in wired and wireless communication projects.